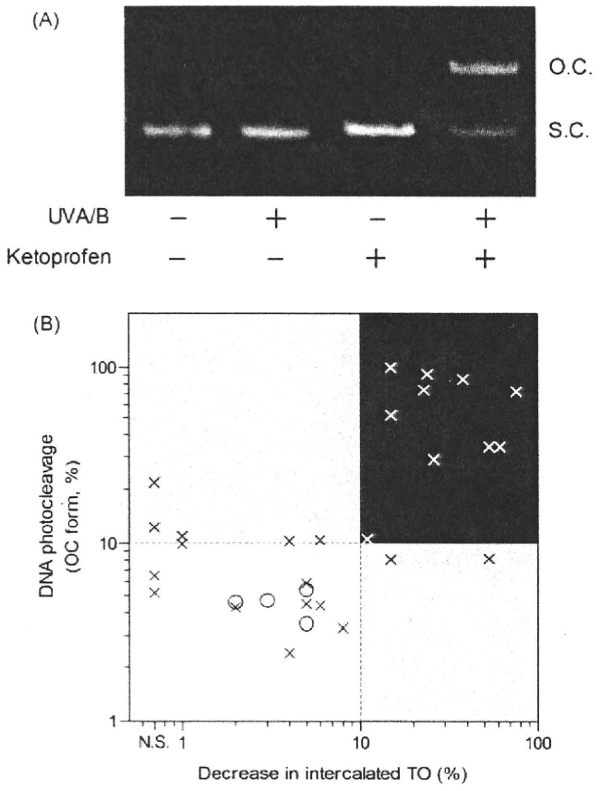

Fig. 3. Photodynamic impairment of DNA induced by irradiated photosensitizers. (A) Ketoprofen-induced photocleavage of plasmid pBR322 DNA. Supercoiled DNA was exposed to UV with or without ketoprofen. EtBr-stained 0.8% agarose gels are shown. OC, open circular form, and SC, supercoiled form. (B) A 2D plot of DNA-photocleavage versus IBP data for 32 compounds. ×, phototoxic drugs; and ○, weak/non-phototoxic drugs. According to tentative classification criteria, plot data were categorized into three regions: (1) shaded region, positive in both assays, (2) gray region, positive in only one assay, and (3) white region, negative in both assays.

lyzed on a 2D plot of generated OC form versus reduced TO intercalation for various pharmaceutical substances (Fig. 3B). With tentative classification criteria (10% DNA damage) to discriminate photogenotoxins from non-photogenotoxic chemicals, plot data were categorized into three regions. Thus, compounds in the shaded region were predicted to be photogenotoxic in both assays, and those predicted to be photogenotoxic by only one assay are plotted in the gray regions. The chemicals for which the photogenotoxic risk might be negligible are in the subthreshold white region. Of all tested compounds, only seven chemicals (22% of the total) were present in the gray regions, that is, they showed a discrepancy between the data from DNA-photocleavage and IBP assays. DNA-photocleavage assay could indicate the impairment of DNA directly, although IBP assay was indicative of decrease in TO-intercalating capacity, reflecting the oxidative DNA damage. The different measuring systems might lead to the data discrepancy between themselves. The 2D-plot analysis suggested that the IBP assay could predict drug-induced DNA damage, reflecting the photogenotoxic potential, with a prediction accuracy of 78%.

Comparative studies of the IBP and DNA-photocleavage assays demonstrated possible limitations of the IBP assay. There is the possibility that the emission of fluorescence from intercalated TO is sometimes quenched by tested compounds or their photodegradants, leading to a limited screening window and misleading results. In the present study, only diclofenac exhibited an extremely limited screening window, suggesting that the photogenotoxic risk of diclofenac might be unpredictable using the IBP assay. For the avoidance of misleading information, the level of intercalated TO in control groups should be compared with that in vehicle groups, which would enable the detection of compounds unsuitable for the IBP assay. However, the IBP assay exhibited some advantages compared with the DNA-photocleavage assay and other photogenotoxic assessment tools such as the CGE analysis [9] and the DNA-binding assay [10]. First, the use of multiwell plates enables the IBP assay to be used to evaluate large numbers of compounds at the same time and to simplify the methodology in preparation and data processing. Second, there is a marked reduction in screening run time compared with that in DNA-photocleavage assay and CGE analysis, because of no electrophoretic process. Last, the DNA-binding assay is not indicative of photogenotoxic risk without ROS data, although the IBP assay does not need them for the risk assessment.

These findings, taken together with those from previous study on ROS assay strategies, indicate that the IBP assay can be employed for detecting the photogenotoxic potential of phototoxic compounds as a 2nd screening tool following the ROS assay, and that this strategy gives more precise and specific prediction of drug-induced photogenotoxicity. The combination of these simplified assay systems would be suitable for evaluating a large number of pharmaceutical candidates and especially effective in early stages of drug discovery.

4. Conclusion

The IBP assay was newly developed for predicting the photogenotoxic potential of pharmaceutical substances. The new assay strategy was found to be more convenient than the prediction tools that we had proposed previously, including the AGE- or CGE-based DNA-photocleavage assay and the DNA-binding assay, with simplified procedures and improved throughput. In this study, we evaluated the photochemical and phototoxic behaviors of 32 model compounds using the ROS assay, the DNA-photocleavage assay, and the IBP assay. Although the results from the IBP assay did not completely correlate with ROS data, the IBP assay exhibited a 78% prediction precision for the oxidative impairment of DNA caused by irradiated drugs. These findings suggest the usefulness of the IBP assay for identifying photogenotoxic risk and avoiding undesired side effects in the early stages of pharmaceutical development. The new assay can be used for screening purposes, and further accumulation of data will allow us to estimate practical classification criteria to identify photogenotoxic chemicals more precisely.

Acknowledgement

This work was supported in part by a Grant-in-Aid from the Food Safety Commission, Japan (No. 0807).

References

[1] J.H. Epstein, Phototoxicity and photoallergy in man, J. Am. Acad. Dermatol. 8 (1983) 141–147.
[2] J.H. Epstein, B.U. Wintroub, Photosensitivity due to drugs, Drugs 30 (1985) 42–57.
[3] S. Onoue, Y. Tsuda, Analytical studies on the prediction of photosensitive/phototoxic potential of pharmaceutical substances, Pharm. Res. 23 (2006) 156–164.
[4] E. Selvaag, A.B. Petersen, R. Gniadecki, T. Thorn, H.C. Wulf, Phototoxicity to diuretics and antidiabetics in the cultured keratinocyte cell line HaCaT: evaluation by clonogenic assay and single cell gel electrophoresis Comet assay), Photodermatol. Photoimmunol. Photomed. 18 (2002) 90–95.
[5] R. Dubakiene, M. Kupriene, Scientific problems of photosensitivity, Medicina (Kaunas) 42 (2006) 619–624.
[6] B. Kersten, P. Kasper, S.Y. Brendler-Schwaab, L. Muller, Use of the photomicronucleus assay in Chinese hamster V79 cells to study photochemical genotoxicity, Mutat. Res. 519 (2002) 49–66.
[7] S. Brendler-Schwaab, A. Czich, B. Epe, E. Gocke, B. Kaina, L. Muller, D. Pollet, D. Utesch, Photochemical genotoxicity: principles and test methods. Report of a GUM task force, Mutat. Res. 566 (2004) 65–91.

[8] S. Onoue, Y. Seto, G. Gandy, S. Yamada, Drug-induced phototoxicity; an early in vitro identification of phototoxic potential of new drug entities in drug discovery and development, Curr. Drug Saf. 4 (2009) 123–136.
[9] S. Onoue, N. Igarashi, F. Kitagawa, K. Otsuka, Y. Tsuda, Capillary electrophoretic studies on the photogenotoxic potential of pharmaceutical substances, J. Chromatogr. A 1188 (2008) 50–56.
[10] S. Onoue, Y. Seto, A. Oishi, S. Yamada, Novel methodology for predicting photogenotoxic risk of pharmaceutical substances based on reactive oxygen species (ROS) and DNA-binding assay, J. Pharm. Sci. 98 (2009) 3647–3658.
[11] W.A. Prutz, Inhibition of DNA-ethidium bromide intercalation due to free radical attack upon DNA. I. Comparison of the effects of various radicals, Radiat. Environ. Biophys. 23 (1984) 1–6.
[12] H.S. Rye, J.M. Dabora, M.A. Quesada, R.A. Mathies, A.N. Glazer, Fluorometric assay using dimeric dyes for double- and single-stranded DNA and RNA with picogram sensitivity, Anal. Biochem. 208 (1993) 144–150.
[13] D.L. Boger, W.C. Tse, Thiazole orange as the fluorescent intercalator in a high resolution fid assay for determining DNA binding affinity and sequence selectivity of small molecules, Bioorg. Med. Chem. 9 (2001) 2511–2518.
[14] S. Onoue, N. Igarashi, S. Yamada, Y. Tsuda, High-throughput reactive oxygen species (ROS) assay: an enabling technology for screening the phototoxic potential of pharmaceutical substances, J. Pharm. Biomed. Anal. 46 (2008) 187–193.
[15] S. Onoue, Y. Yamauchi, T. Kojima, N. Igarashi, Y. Tsuda, Analytical studies on photochemical behavior of phototoxic substances; effect of detergent additives on singlet oxygen generation, Pharm. Res. 25 (2008) 861–868.
[16] A.R. Morgan, D.E. Pulleyblank, Native and denatured DNA, cross-linked and palindromic DNA and circular covalently-closed DNA analysed by a sensitive fluorometric procedure, Biochem. Biophys. Res. Commun. 61 (1974) 396–403.

Journal of Pharmaceutical and Biomedical Analysis 55 (2011) 591–596

Contents lists available at ScienceDirect

Journal of Pharmaceutical and Biomedical Analysis

journal homepage: www.elsevier.com/locate/jpba

In vitro photobiochemical characterization of sulfobutylether-β-cyclodextrin formulation of bufexamac

Yoshiki Seto [a], Masanori Ochi [a], Naoko Igarashi [b], Ryo Inoue [a], Ami Oishi [a], Toshihiko Toida [b], Shizuo Yamada [a], Satomi Onoue [a,*]

[a] *Department of Pharmacokinetics and Pharmacodynamics and Global Center of Excellence (COE) Program, School of Pharmaceutical Sciences, University of Shizuoka, 52-1 Yada, Suruga-ku, Shizuoka 422-8526, Japan*

[b] *Graduate School of Pharmaceutical Sciences, Chiba University, 1-8-1 Inohana, Chuo-ku Chiba 260-8675, Japan*

ARTICLE INFO

Article history:
Received 13 January 2011
Received in revised form 16 February 2011
Accepted 19 February 2011
Available online 26 February 2011

Keywords:
Reactive oxygen species assay
Photoreactivity
Bufexamac
Sulfobutylether-β-cyclodextrin
Inclusion complex

ABSTRACT

The present study aimed to modulate the photoreactivity of bufexamac, with a focus on photostability and phototoxicity, by forming an inclusion complex with sulfobutylether-β-cyclodextrin (SBECD). The photobiochemical properties of bufexamac were evaluated by reactive oxygen species (ROS) assay and using *in vitro* photogenotoxic assessment tools. To assess the inclusion properties of SBECD complex with bufexamac, a UV absorption spectroscopic study was also carried out. The influence of SBECD on the photoreactivity of bufexamac was analyzed by ROS assay and photostability test. From the photobiochemical data, superoxide generation from irradiated bufexamac indicated its photoreactivity; however, the photogenotoxic risk of bufexamac was negligible owing to low DNA-binding affinity and DNA-photocleaving activity. SBECD complex of bufexamac was formed, and the association constant of the complex was calculated to be 620 M^{-1}. On the basis of the photochemical data on bufexamac co-existing with SBECD, ROS generation from irradiated bufexamac (200 μM) was inhibited by SBECD at concentrations of over 20 μM. The degradation constant of bufexamac in SBECD was decreased ca. 30% compared with that of bufexamac, suggesting improvement of its photostability. The phototoxic risk of bufexamac might be attenuated by SBECD complexation, and cyclodextrin inclusion complexes might be a useful approach for modulating the phototoxicity of drugs.

1. Introduction

Photochemical reactions of pharmaceutics, including photodegradation and phototoxicity, are severe problems in terms of stability and safety in the pharmaceutical industry, and their possible cascade has been reported [1,2]. Drugs are excited by UVA (320–400 nm) and UVB (290–320 nm), and then the drugs directly/indirectly react with molecules, resulting in photodegradation and phototoxicity [1]. Reactive oxygen species (ROS) have been reported as one of the major causative intermediate species for photochemical reactions [3], and the ROS generation from irradiated chemicals induce the oxidation of various molecules. Notably, excited compounds react with biomolecules, leading to phototoxic skin responses, including photoirritation, photoallergy, and photogenotoxicity [1,4]. Several classes of pharmaceuticals, such as diuretic agents [5], non-steroidal anti-inflammatory drugs (NSAIDs) [6], and tricyclic antidepressants [7], exhibit some or all of the phototoxic reactions. Recently, for evaluating the photoreactivity of pharmaceutics, a ROS assay was proposed as a new photochemical assessment tool [1,8] to monitor ROS generation from irradiated compounds, including both singlet oxygen and superoxide. There appeared to be a good relationship between ROS generation and occurrences of phototoxic events for a number of known phototoxic compounds [8].

In previous studies, inclusion complexes of drugs with cyclodextrins (CyDs) were used for modulating the photoreactivity of pharmaceutics, such as naproxen, amlodipine, flutamide and curcuminoids [9–12]. Notably, phototoxic skin reactions of topically administered drugs are a critical hazard, and the adverse effects should be avoided. Thus, CyD complexations might modulate the phototoxic risk of topically administered compounds. Bufexamac, the model compound in the present study (Fig. 1), is administered topically on the skin in clinical use; however, phototoxic skin event of bufexamac has been reported [13]. The purpose of the present study was to control the phototoxic potential of bufexamac by using complexation with sulfobutylether-β-cyclodextrin (SBECD), a β-CyD derivative. The photochemical behavior of bufexamac was assessed by ROS assay. For assessment of photogenotoxic potential, the interaction of bufexamac with DNA was assessed by circular dichroism (CD) analysis and DNA-binding assay [14] and

* Corresponding author. Tel.: +81 54 264 5633; fax: +81 54 264 5635.
E-mail address: onoue@u-shizuoka-ken.ac.jp (S. Onoue).

0731-7085/$ – see front matter © 2011 Elsevier B.V. All rights reserved.
doi:10.1016/j.jpba.2011.02.025

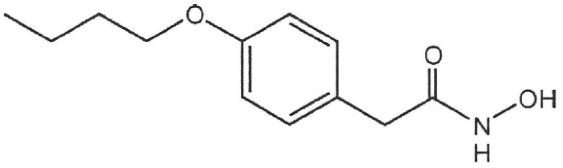

Fig. 1. Structure of bufexamac.

bufexamac-induced DNA photocleavage was evaluated by agarose gel electrophoresis. SBECD inclusion complex of bufexamac was formed and its inclusion properties were estimated using a spectroscopic study [15]. Possible changes of the photoreactivity of bufexamac with SBECD were evaluated by ROS assay, and the photostability of bufexamac with or without SBECD was monitored by ultra performance liquid chromatography equipped with electrospray ionization mass spectrometry (UPLC/ESI-MS).

2. Materials and methods

2.1. Chemicals

Bufexamac was purchased from Sigma (St. Louis, MO, USA). SBECD was supplied by Pfizer Inc. Salmon sperm DNA, plasmid pBR322 DNA, imidazole, p-nitrosodimethylaniline (RNO), nitroblue tetrazolium (NBT), Tween 20, disodium hydrogenphosphate 12-water, and sodium dihydrogenphosphate dihydrate were obtained from Wako Pure Chemical Industries (Osaka, Japan). Ethidium bromide (EtBr) and agarose L03 were purchased from Nippon Gene (Toyama, Japan) and Takara Bio (Shiga, Japan), respectively. Acetonitrile was purchased from Kanto Chemical (Tokyo, Japan). A quartz reaction container for high-throughput ROS assay was constructed by Ozawa Science (Aichi, Japan).

2.2. Determination of reactive oxygen species (ROS)

Singlet oxygen was determined following the Kraljic and ElMoshni procedure [16]. Briefly, samples containing bufexamac with or without SBECD, RNO (50 μM), and imidazole (50 μM) in 20 mM sodium phosphate buffer (NaPB, pH 7.4) were irradiated with UVA/B (30,000 lx) in a Light-Tron Xenon (LTX-01, Nagano Science, Osaka, Japan), and then UV absorption at 440 nm was measured using a SpectraMax plus 384 microplate spectrophotometer (Molecular Devices, Kobe, Japan).

Superoxide anion was also determined according to the Pathak and Joshi procedure [17]. Samples containing bufexamac (free or in SBECD inclusion complex) and NBT (50 μM) in 20 mM NaPB (pH 7.4) were irradiated with UVA/B (30,000 lx) for the indicated periods, and the reduction of NBT was measured by the increase of their absorbance at 560 nm, using SpectraMax plus 384 microplate spectrophotometer.

2.3. Circular dichroism (CD) analysis of DNA

Salmon sperm DNA with or without bufexamac was dissolved in 20 mM NaPB (pH 7.4), and CD spectra (average of ten scans) were collected from samples (2.4 mL) at 0.4 nm intervals between wavelengths of 200 and 350 nm using a Jasco model J-600 spectropolarimeter. Measurement was carried out at room temperature, and a baseline spectrum was subtracted from the collected data.

2.4. DNA-binding assay

The affinity of drugs for salmon sperm DNA was determined by the competitive binding study. For competitive binding experiments, 10 μL of DNA solution at a concentration of 100 μg/mL, dissolved in 20 mM NaPB (pH 7.4), was mixed with 20 μL of the tested drug at various final concentrations ranging from 0 to 2 μM in a 96-well microplate (AGC TECHNO GLASS, Chiba, Japan), then 70 μL of EtBr (7.0 μM) was added to the assay mixture. The mixture was incubated for 15 min at 37 °C. After incubation, the fluorescence (excitation, 550 nm, and emission, 590 nm) of each mixture (100 μL) in 96-well microplates was measured with a Multilabel Counter (PerkinElmer, Norwalk, CT, USA).

2.5. DNA-photocleavage assay

The sample containing pBR322 DNA (10 μg/mL) and bufexamac (200 μM) in Tris–acetic acid–EDTA (TAE) buffer (40 mM Tris, 20 mM acetic acid, and 1 mM EDTA) was irradiated with UVA/B (375 kJ/m^2) in an Atlas Suntest CPS+ solar simulator (Atlas Material Technology LLC, Chicago, USA) equipped with a xenon arc lamp (1500 W). After the irradiation test, irradiated plasmid pBR322 DNA was separated by electrophoresis (0.8% agarose gel in TAE buffer), visualized with EtBr staining, and analyzed with image analyzing software Image J.

2.6. Determination of stoichiometry and the association constant

Bufexamac (0.5 mM) was dissolved in 20 mM NaPB (pH 7.4) containing 5% acetonitrile with SBECD (5, 10, 15, 20, 25, and 30 mM). Solutions containing the same concentrations of SBECD without bufexamac were also prepared. UV–Vis absorption spectra were recorded with a HITACHI U-2010 spectrophotometer (HITACHI, Tokyo, Japan) interfaced to a PC for data processing (Software: Spectra Manager). Spectrofluorimeter quartz cell with 10 mm pathlength was employed. The spectra of bufexamac were obtained by the subtraction of the spectra of SBECD from those of complex for removal of the contribution of SBECD. The obtained UV absorption of bufexamac at 278 nm (A_{278}) was substituted into the following Scott's equation, and described on Scott's plot [15]:

$$[\text{SBECD}] \cdot [\text{Buf}] \cdot \frac{L}{A_{278}} = \frac{1}{\varepsilon}[\text{SBECD}] + \frac{1}{K \cdot \varepsilon}$$

where [SBECD] and [Buf] indicate the molar concentrations of SBECD and bufexamac (mM), respectively. L is the light path length, ε equals to the molar extinction coefficient, and K represents the association constant. Then, the values of K and stoichiometry were obtained from Y-intercept/slope and linearity of Scott's plot, respectively.

2.7. Photostability testing

For photostability testing, the solutions of bufexamac (1 mg/mL) and its SBECD inclusion complex (equimolar ratio between bufexamac and SBECD) were dissolved in water containing 50% acetonitrile in a 1.5 mL clear glass vial (12 mm × 32 mm, Shimadzu, Kyoto, Japan). The samples were stored in the Atlas Suntest CPS+ solar simulator, and photostability testing was carried out at 25 °C with an irradiance of 750 W/m^2 for the indicated times (0, 15, 30, 60, and 120 min). The irradiated and non-irradiated samples were subjected to UPLC analyses to determine the amounts of remaining bufexamac. All analyses were performed on a Waters Aquity UPLC™ system (Waters, Milford, MA), which includes a binary solvent manager, a sample manager, a column compartment, and a Micromass SQ detector connected with a Waters Masslynx v 4.1. A Waters Acquity UPLC™ BEH C_{18} (particle size: 1.7 μm, column size: ϕ2.1 mm × 50 mm; Waters) was used, and the column temperature was maintained at 40 °C. The standards and samples were separated using a gradient mobile phase consisting of Milli-Q containing 0.1% formic acid (A) and methanol (B). The gradient condition of

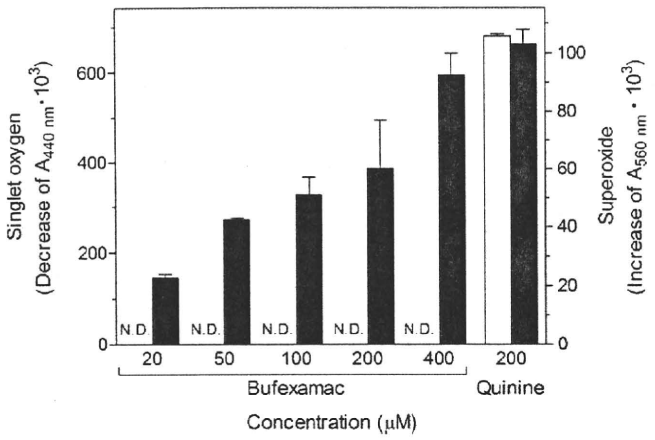

Fig. 2. Generation of ROS from photoirradiated bufexamac and quinine. Each chemical was dissolved in 20 mM NaPB (pH 7.4) at the indicated concentrations, and then exposed to simulated sunlight (30,000 lx). Open bar, singlet oxygen; and filled bar, superoxide. Data represent mean ± S.D. of three experiments.

the mobile phase was 0–0.5 min, 50% A; 0.5–3.5 min, 50–5% A; 3.5–5 min, 5%, and the flow rate was set at 0.25 mL/min.

2.8. Data analysis

For statistical comparisons, a one-way analysis of variance (ANOVA) with the pairwise comparison by Fisher's least significant difference procedure was used. A P value of less than 0.05 was considered significant for all analyses.

3. Results

3.1. Photochemical reactions of bufexamac

The ROS assay enabled to identification of the type of photochemical reaction by monitoring the generation of singlet oxygen through type II photochemical reaction and superoxide through type I photochemical reaction. In the present study, the generation of ROS from bufexamac was detected by ROS assay to clarify the type of photochemical reaction for bufexamac (Fig. 2). Exposure of quinine, a known phototoxic drug, to simulated sunlight resulted in the generation of both singlet oxygen and superoxide; however, bufexamac could generate only superoxide in a concentration-dependent manner. The results suggested that bufexamac would mainly induce type I photochemical reaction. The ROS-generating behavior of bufexamac ($^1O_2$, $\Delta_{440} \times 10^3$: not detected, O_2^-, $\Delta_{560} \times 10^3$: 60) was similar to that of carbamazepine ($^1O_2$, $\Delta_{440} \times 10^3$: not detected, O_2^-, $\Delta_{560} \times 10^3$: 96), a phototoxic drug [18], at a concentration of 200 μM [19]. Thus, bufexamac was found to be photoreactive and/or phototoxic, and the result was in agreement with a previous clinical report [13].

3.2. Photogenotoxic potential of bufexamac

For further photochemical characterization, the interaction of bufexamac with DNA was evaluated by DNA-binding assay [14], and nalidixic acid, which has the affinity to DNA, was used as a positive control (Fig. 3A). The emission of intense fluorescence from ethidium (4.9 μM) was observed in the presence of DNA (10 μg/mL). The addition of nalidixic acid induced a decrease of fluorescence in a concentration-dependent manner; however, no significant changes of fluorescence emission were observed for bufexamac, suggesting low affinity of bufexamac to DNA. To clarify the interaction of bufexamac and DNA, CD spectral analysis on DNA

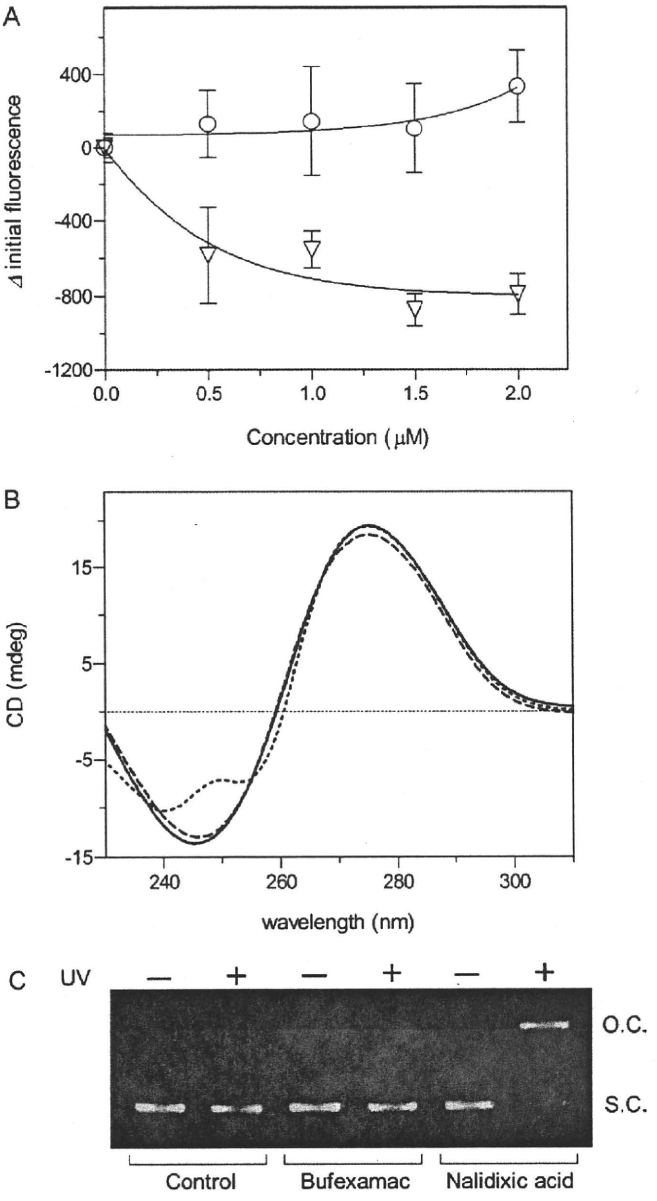

Fig. 3. *In vitro* photogenotoxic assessments. (A) Typical ethidium displacement curves for chemicals. The binding of ethidium (4.9 μM) to DNA was inhibited by increasing concentrations of nalidixic acid, but not by bufexamac. (○) Bufexamac and (▽) nalidixic acid. Data represent mean ± S.D. of four experiments. (B) CD spectra representative of DNA (100 μg/mL) in the presence of compounds (100 μM). Solid line, DNA alone; dashed line, DNA in the presence of bufexamac; and dotted line, DNA in the presence of nalidixic acid. (C) Photodynamic impairment of plasmid pBR322 DNA induced by irradiated compounds. Supercoiled DNA was exposed to UV with/without compounds. EtBr-stained 0.8% agarose gels are shown. O.C., open circular form; and S.C., supercoiled form.

(100 μg/mL) with or without compounds (100 μM) was also carried out (Fig. 3B). A solution of DNA exhibits a positive band at 275 nm due to base stacking and a negative band at 248 nm due to the helicity, which is characteristic of DNA in the right-handed B form [20]. Adding nalidixic acid to DNA solution, the intensity of the negative band at 248 nm decreased, suggesting the structural changes of DNA. In contrast, no spectral transitions were observed for bufexamac, suggesting weak interaction of bufexamac with DNA.

To validate the photogenotoxic risk of bufexamac, the conversion of plasmid pBR322 DNA from supercoiled (SC) form to open circular (OC) form was also analyzed by AGE (Fig. 3C). DNA damage

was clearly induced by nalidixic acid after exposure to simulated sunlight, and the conversion of pBR322 DNA from the SC to the OC form was estimated to be ca. 64% on the basis of the band intensity. In contrast, bufexamac-induced DNA photocleavage was not observed, suggesting that bufexamac is less photogenotoxic. Overall, bufexamac exhibited neither interaction with DNA nor DNA-photocleaving activity, and bufexamac may not cause photogenotoxicity.

3.3. Stoichiometric analysis of bufexamac–SBECD inclusion complex

The photobiochemical data of bufexamac indicated photodegradative and phototoxic potentials, except photogenotoxic risk, and SBECD complexation was applied for modulating the photoreactivity of bufexamac in this study. Generally, there is an optimal molar ratio between CyD and chemicals for forming an inclusion complex; therefore, a spectroscopic method using the changes of UV-absorption spectra and Scott's plot was used for evaluating the stoichiometry of the inclusion complex in the present investigation [15]. The UV spectral patterns of SBECD–bufexamac complex were recorded in 20 mM NaPB (pH 7.4) (Fig. 4A). On the basis of UV spectral data, hyperchromicity and slight bathochromicity were observed ranging from 250 nm to 300 nm, and strong absorption was detected at approximately 278 nm; these effects suggested that the UV absorbability of bufexamac was changed by SBECD. To obtain the stoichiometry and association constant of the SBECD inclusion complex of bufexamac, Scott's plot was described using the UV absorption data and the concentrations of bufexamac and SBECD (Fig. 4B). The plot of SBECD concentration versus [SBECD]·[Buf]/Absorbance exhibited linearity, and its correlation coefficient was estimated to be 1.00. Generally, the inclusion ratio between CyD and compound is stoichiometrically determined to be 1:1 when Scott's plot is indicative of the linearity [21]. In addition to the stoichiometry of the inclusion complex, the value of K of the inclusion complex was also calculated to be 620 M^{-1} from the present analysis. On the basis of the data obtained, SBECD forms a 1:1 inclusion complex with bufexamac, and the complex should be relatively stable.

3.4. Inhibitory effect of SBECD on ROS generation from bufexamac

Although SBECD complex with bufexamac could be formed, the influence of SBECD on the photochemical behavior of bufexamac is still unclear. Therefore, ROS generation from irradiated bufexamac (200 μM) co-existing with SBECD (ranging from 0 to 800 μM) was examined by ROS assay to clarify the possible transition of photoreactivity for bufexamac (Fig. 5). SBECD complexation led to suppression of superoxide generation from irradiated bufexamac in an SBECD-concentration-dependent manner. In detail, SBECD at concentrations of 20 and 100 μM exhibited significant reduction of superoxide generation from irradiated bufexamac by ca. 75 and 92%, respectively, and the generation of superoxide was negligible in the presence of SBECD at concentration of over 200 μM. On the basis of the data obtained, SBECD modulated the photoreactivity of bufexamac by forming an inclusion complex, and SBECD may attenuate bufexamac-induced phototoxic skin reactions by forming an inclusion complex when the complex is topically administered.

3.5. Photostability testing on bufexamac and its SBECD-inclusion complex

According to the ROS data, photoreactive and/or phototoxic potential of bufexamac is modulated by SBECD; this finding prompted us to clarify the photostability of bufexamac in SBECD. Solution-state photostability test using a solar simulator was

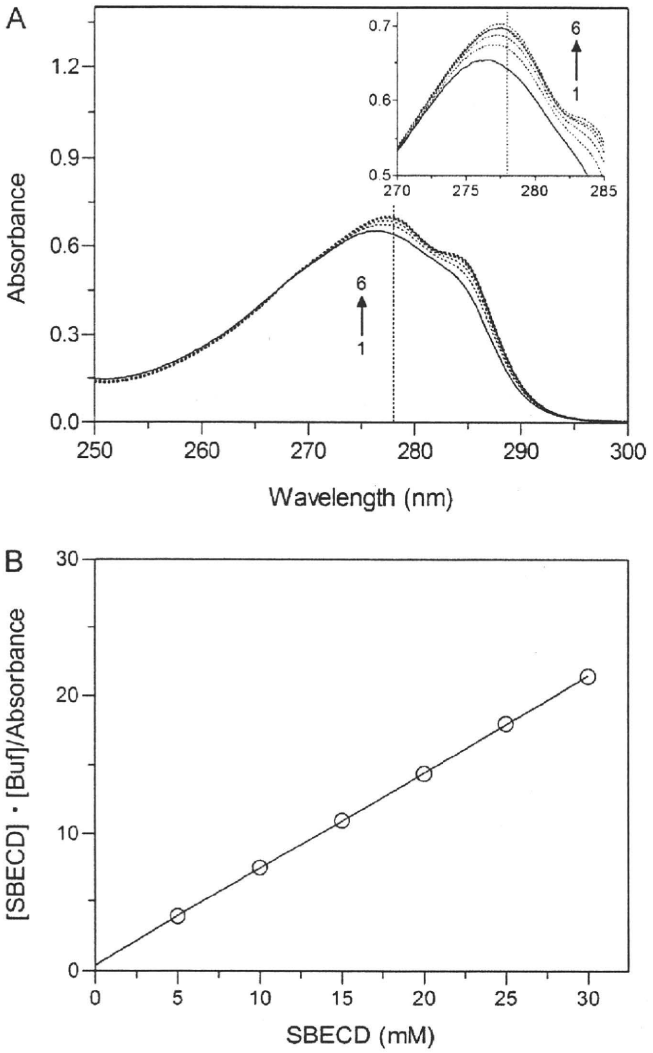

Fig. 4. Stoichiometry analysis of SBECD inclusion property for bufexamac. (A) UV spectral patterns of bufexamac (0.5 mM) with SBECD. Concentration of SBECD: (1) 5, (2) 10, (3) 15, (4) 20, (5) 25, and (6) 30 mM. (1) Solid line; (2)–(6) dotted line. (B) Scott's plot for interaction between bufexamac and SBECD by UV spectrometry.

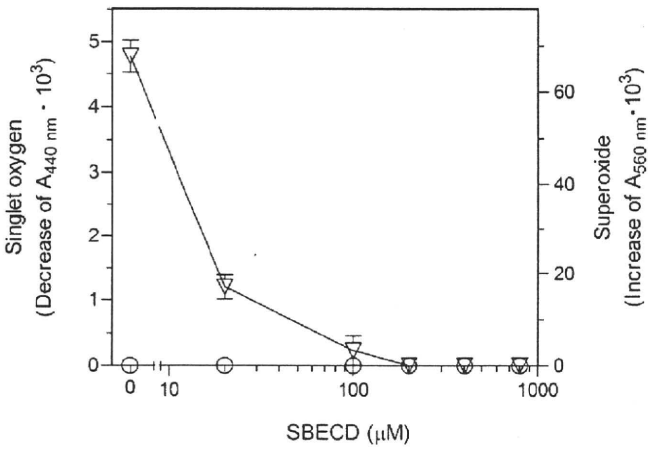

Fig. 5. Generation of ROS from irradiated inclusion complex of bufexamac with SBECD. SBECD was dissolved in 20 mM NaPB (pH 7.4) at the indicated concentrations with bufexamac (200 μM), and then exposed to simulated sunlight (30,000 lx). (○) singlet oxygen; and (▽) superoxide. Data represent mean ± S.D. of three experiments.

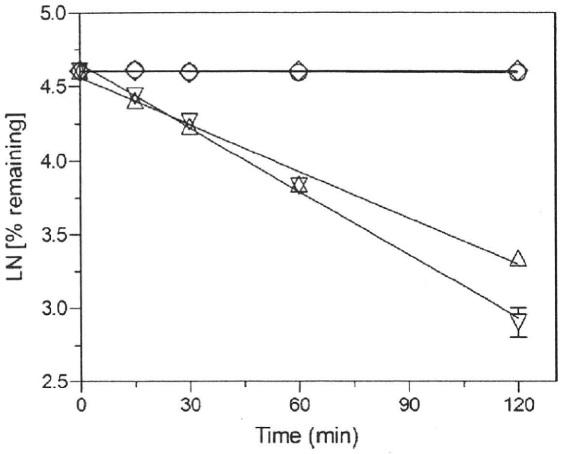

Fig. 6. Photodegradation profiles of bufexamac. Each sample was exposed to UVA/B (750 W/m^2) for the indicated periods, and the remaining bufexamac was evaluated by UPLC/ESI-MS. Bufexamac: (○) non-irradiated, and (▽) irradiated, and bufexamac-SBECD inclusion complex: (◇) non-irradiated, and (△) irradiated. Data represent mean ± S.D. of three experiments.

carried out on bufexamac with or without SBECD (Fig. 6). Degradation kinetics was calculated according to the following equation: $\ln A = \ln A_0 - kt$, where A is the remaining peak area of bufexamac, t is the time (min), and k is the slope (degradation constant). Both bufexamac solutions were stable without UV irradiation since the results of the remaining bufexamac were estimated to be almost 100% of initial bufexamac until 120 min in both bufexamac solutions. In contrast, solution-state bufexamac was rapidly photodegraded by exposure to UV, and the remaining bufexamac at 120 min was estimated to be ca. 18.3%. The solution-state bufexamac in SBECD was also photodegraded after UV irradiation, and the remaining bufexamac at 120 min was calculated to be ca. 28.2%. The degradation constants of bufexamac with and without SBECD were estimated to be 1.05×10^{-2} min^{-1} and 1.43×10^{-2} min^{-1}, respectively. There was ca. 30% reduction of the degradation constant of bufexamac by forming SBECD complexation; therefore, the photostability of bufexamac should be slightly improved by SBECD.

4. Discussion

In the present study, we first demonstrated that SBECD complexation was effective for controlling the phototoxicity of bufexamac. On the basis of the photobiochemical data, bufexamac generated superoxide; however, the photogenotoxic potential of bufexamac was not identified. SBECD inclusion complex of bufexamac was prepared, and the inclusion ratio was estimated to be 1:1 by a spectroscopic method. From the photochemical data on the inclusion complex, the photoreactivity of bufexamac might be modulated by equimolar SBECD.

Generally, CyDs are often applied for improving solubility, dissolution rate, bioavailability, and chemical stability, including hydrolysis oxidation and photodegradation of drugs [22,23]. In particular, β-CyD is considered a useful solubilizing agent because of its inclusion abilities; however, natural β-CyD has limited aqueous solubility due to relatively strong binding of the CyD molecules. To overcome this drawback, SBECD, an anionic β-CyD derivative, was synthesized for better solubilization than natural β-CyD, and it has been applied as a solubilizing agent for some pharmaceutics, such as ziprasidone, aripiprazole, and voriconazole [24].

On the basis of the ROS data, bufexamac was found to have photoreactivity, possibly leading to photodegradation and phototoxicity; however, the potent photogenotoxic risk of bufexamac was not observed in all the *in vitro* photogenotoxic assessment tools. Although the photogenotoxic risk of bufexamac was negligible, bufexamac should be indicative of photoreactivity mainly via type I photochemical reaction since bufexamac is topically used in clinical settings, and the phototoxic risk of bufexamac is recognized as one of its severe side effects. To attenuate the phototoxic potential of bufexamac, SBECD-based formulation was designed in the present investigation. On the basis of the physicochemical data, SBECD should form equimolar and stable inclusion complex with bufexamac. Photochemical properties of the inclusion complex were examined to clarify whether SBECD truly attenuated the phototoxicity of bufexamac. On the basis of the ROS data, generation of superoxide from bufexamac was completely inhibited by more than an equimolar concentration of SBECD. The photostability of bufexamac was also improved slightly by forming inclusion complex with SBECD owing to the ca. 30% reduction of the degradation constant of bufexamac. The results suggest that SBECD attenuated photoactivation of bufexamac and/or blocked interaction of excited bufexamac with oxygen owing to complexation with bufexamac. Overall, bufexamac in SBECD was found to be less photoreactive than bufexamac itself, and SBECD-based complexation might be effective for modulating the phototoxicity of bufexamac in terms of photosafety.

Topical application of chemicals on the skin provokes the concern about the occurrence of the phototoxic risk of the compounds because of direct exposure of the skin to both compounds and sunlight. Previously, Moore et al. reported that topically applied agents, such as ketoprofen, coumarin, and hydrocortisone, induced direct cutaneous phototoxicity [25]. According to the European Medicines Agency (EMEA) and the Food and Drug Administration (FDA) guidelines [26–28], topical application of compounds has been explicitly described as one of the conditions for testing chemicals; therefore, attenuation of the phototoxic risk of topically applied chemicals is required in terms of photosafety. Sunscreens are usually used to avoid drug-induced photodermatoses [25], and the present investigation suggested that CyD complexation may also be an effective approach for controlling the phototoxicity of topically administered drugs.

In conclusion, SBECD could inhibit ROS generation from irradiated bufexamac and slightly improve the photostability of bufexamac; therefore, the phototoxic risk of bufexamac could be reduced by SBECD complexation, and the SBECD-based formulation strategy might be effective for modulating the phototoxicity of bufexamac.

Acknowledgements

This work was supported in part by a Grant-in-Aid from the Food Safety Commission, Japan [No. 0807] and a Health Labour Sciences Research Grant from The Ministry of Health, Labour and Welfare, Japan.

References

[1] S. Onoue, Y. Tsuda, Analytical studies on the prediction of photosensitive/phototoxic potential of pharmaceutical substances, Pharm. Res. 23 (2006) 156–164.
[2] S. Onoue, Y. Seto, G. Gandy, S. Yamada, Drug-induced phototoxicity; an early *in vitro* identification of phototoxic potential of new drug entities in drug discovery and development, Curr. Drug Saf. 4 (2009) 123–136.
[3] C.S. Foote, Definition of type I and type II photosensitized oxidation, Photochem. Photobiol. 54 (1991) 659.
[4] D.E. Moore, Mechanisms of photosensitization by phototoxic drugs, Mutat. Res. 422 (1998) 165–173.
[5] F. Vargas, I. Martinez Volkmar, J. Sequera, H. Mendez, J. Rojas, G. Fraile, M. Velasquez, R. Medina, Photodegradation and phototoxicity studies of furosemide. Involvement of singlet oxygen in the photoinduced hemolysis and lipid peroxidation, J. Photochem. Photobiol. B 42 (1998) 219–225.

[6] L. Becker, B. Eberlein-Konig, B. Przybilla, Phototoxicity of non-steroidal anti-inflammatory drugs: *in vitro* studies with visible light, Acta Derm. Venereol. 76 (1996) 337–340.
[7] G. Viola, G. Miolo, D. Vedaldi, F. Dall'Acqua, *In vitro* studies of the phototoxic potential of the antidepressant drugs amitriptyline and imipramine, Farmaco 55 (2000) 211–218.
[8] S. Onoue, K. Kawamura, N. Igarashi, Y. Zhou, M. Fujikawa, H. Yamada, Y. Tsuda, Y. Seto, S. Yamada, Reactive oxygen species assay-based risk assessment of drug-induced phototoxicity: classification criteria and application to drug candidates, J. Pharm. Biomed. Anal. 47 (2008) 967–972.
[9] M. Partyka, B.H.A.H. Evans, Cyclodextrins as phototoxicity inhibitors in drugs formulation; studies on model systems involving naproxen and β-cyclodextrin, J. Photochem. Photobiol. A: Chem. 140 (2001) 67–74.
[10] G. Ragno, E. Cione, A. Garofalo, G. Genchi, G. Ioele, A. Risoli, A. Spagnoletta, Design and monitoring of photostability systems for amlodipine dosage forms, Int. J. Pharm. 265 (2003) 125–132.
[11] S. Sortino, S. Petralia, G. Condorelli, G. Marconi, Direct spectroscopic evidence that the photochemical outcome of flutamide in a protein environment is tuned by modification of the molecular geometry: a comparison with the photobehavior in cyclodextrin and vesicles, Helv. Chim. Acta 86 (2003) 266–273.
[12] M.A. Tomren, M. Masson, T. Loftsson, H.H. Tonnesen, Studies on curcumin and curcuminoids. XXXI. Symmetric and asymmetric curcuminoids: stability, activity and complexation with cyclodextrin, Int. J. Pharm. 338 (2007) 27–34.
[13] Y. Kurumaji, Photo Koebner phenomenon in erythema-multiforme-like eruption induced by contact dermatitis due to bufexamac, Dermatology 197 (1998) 183–186.
[14] S. Onoue, Y. Seto, A. Oishi, S. Yamada, Novel methodology for predicting photogenotoxic risk of pharmaceutical substances based on reactive oxygen species (ROS) and DNA-binding assay, J. Pharm. Sci. 98 (2009) 3647–3658.
[15] R.L. Scott, Some comments on the Benesi–Hildebrand equation, Rec. Trav. Chim. Pays B 75 (1956) 787–789.
[16] I. Kraljic, S.E. Mohsni, A new method for the detection of singlet oxygen in aqueous solutions, Photochem. Photobiol. 28 (1978) 577–581.
[17] M.A. Pathak, P.C. Joshi, Production of active oxygen species ($^1O_2$ and O_2^-.) by psoralens and ultraviolet radiation (320–400 nm), Biochim. Biophys. Acta 798 (1984) 115–126.
[18] T. Terui, H. Tagami, Eczematous drug eruption from carbamazepine: coexistence of contact and photocontact sensitivity, Contact Dermatitis 20 (1989) 260–264.
[19] S. Onoue, M. Ochi, G. Gandy, Y. Seto, N. Igarashi, Y. Yamauchi, S. Yamada, High-throughput screening system for identifying phototoxic potential of drug candidates based on derivatives of reactive oxygen metabolites, Pharm. Res. 27 (2010) 1610–1619.
[20] V.I. Ivanov, L.E. Minchenkova, A.K. Schyolkina, A.I. Poletayev, Different conformations of double-stranded nucleic acid in solution as revealed by circular dichroism, Biopolymers 12 (1973) 89–110.
[21] M. Otagiri, K. Uekama, K. Ikeda, Inclusion complexes of beta-cyclodextrin with tranquilizing drugs phenothiazines in aqueous solution, Chem. Pharm. Bull. 23 (1975) 188–195.
[22] T. Loftsson, M.E. Brewster, Pharmaceutical applications of cyclodextrins. 1. Drug solubilization and stabilization, J. Pharm. Sci. 85 (1996) 1017–1025.
[23] S. Scalia, R. Tursilli, N. Sala, V. Iannuccelli, Encapsulation in lipospheres of the complex between butyl methoxydibenzoylmethane and hydroxypropyl-beta-cyclodextrin, Int. J. Pharm. 320 (2006) 79–85.
[24] D.R. Luke, K. Tomaszewski, B. Damle, H.T. Schlamm, Review of the basic and clinical pharmacology of sulfobutylether-beta-cyclodextrin (SBECD), J. Pharm. Sci. 99 (2010) 3291–3301.
[25] D.E. Moore, Drug-induced cutaneous photosensitivity: incidence, mechanism, prevention and management, Drug Saf. 25 (2002) 345–372.
[26] The European Agency for the Evaluation of Medicinal Products, Evaluation of Medicines for Human Use, Committee for Proprietary Medicinal Products, Note for Guidance on Photosafety Testing, CPMP/SWP/398/01, 2002.
[27] The European Agency for the Evaluation of Medicinal Products, Evaluation of Medicines for Human Use, Committee for Proprietary Medicinal Products, Concept Paper on the Need for Revision of the Note for Guidance on Photosafety Testing, CPMP/SWP/398/01, 2008.
[28] United States Department of Health and Human Services, Food and Drug Administration, Center for Drug Evaluation and Research (CDER) Guidance for Industry, Photosafety Testing, 2002.

薬剤性光線過敏症
創薬初期スクリーニングからレギュレーションまで

尾上誠良
Satomi ONOUE
静岡県立大学薬学部薬物動態学分野准教授

1 はじめに

ヒトに投薬された医薬品が体内で光と相互作用を起こした結果，主に皮膚において誘発される有害反応を薬剤性光線過敏症という．それほど頻繁に耳にする副作用ではないが，2009年度の我が国における売り上げ上位5製品のうち4品目において，光線過敏症の副作用が認められている興味深い事実は，多くの患者が潜在的に本副作用に直面している可能性を示唆するものであろう．このような外因性の光線過敏症はごく最近になって見いだされた新しい副作用ではなく，ある種の植物が同様の毒性作用を示すことが紀元前から知られていたようである．※ 医薬品の安全性に関する近年の高い関心とあいまって，創薬従事者にとっては国際的なレベルで標準化された光安全性評価方法の開発が急務の課題の1つとなっている．本稿では，薬剤性光線過敏症の種類や機序などの基本的な情報とレギュラトリーサイエンス上の光安全性評価方法を紹介するとともに，筆者らが現在取り組んでいる創薬初期過程における光毒性スクリーニングツール開発について併せて紹介したい．

2 光線過敏症の種類と機序

光線過敏症は皮膚において多様な反応を示すが，それらは(i)光曝露中の発赤，(ii)遅延型皮膚炎，(iii)異常な皮膚角質化ならびに細胞の空胞化，(iv)皮膚の落屑などである．薬剤性光線過敏症の原因となる医薬品は既に多く特定されているが，[2,3] 特に抗菌剤，抗ヒスタミン薬，向精神薬，利尿薬，消炎鎮痛薬の一部において顕著な光毒性を認めることがある(表1)．[3] 光線過敏症リスク回避を考える上で光線過敏症を誘発しやすい母骨格や発色団構造についてはしばしば議論の対象となり，創薬においても活発な構造-毒性相関研究が展開されている．その中の成功事例としてニューキノロンがよく知られており，8位のハロゲンが光反応性に強く寄与していることが解明され，なおかつ，それをメトキシ基に置換することでガチフロキサシンのように光線過敏症リスクが低い抗菌剤の創製に成功している．[4] 合成

表1 薬剤性光線過敏症が報告されている医薬品の一例

分類		薬剤名
抗菌剤	キノロン系	シプロフロキサシン，ノルフロキサシン，ナリジクス酸
	テトラサイクリン系	ドキシサイクリン，ミノサイクリン，オキシテトラサイクリン
抗ヒスタミン薬		ジフェンヒドラミン，メキタジン
向精神薬		クロルプロマジン，ハロペリドール，イミプラミン
降圧薬		ジルチアゼム，カプトプリル，ニフェジピン
利尿薬		アセタゾラミド，クロロチアジド，フロセミド
抗糖尿病薬		グリベンクラミド，トルブタミド，クロルプロパミド
消炎鎮痛薬		ジクロフェナク，イブプロフェン，インドメタシン，ナプロキセン

※ 植物の光毒性とそれを利用した光線療法が，古代エジプトやインドで行われていたことが記載されている．[1] これ以外にも，バビロンやギリシャ等の記述が他論文にある．

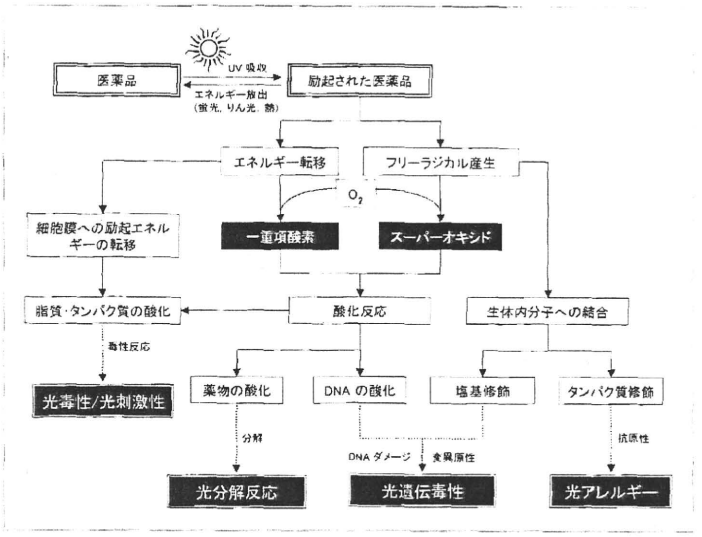

図1　薬剤性光線過敏症の発生機序

医薬品のみならず，漢方，民間療法薬，そしてハーブ類も同様の光線過敏症を惹起することがよく知られており，特にセリ科，ミカン科，オトギリソウ科植物などで観察される．これらの中には，St. John's wort (*Hypericum perforatum*) やベルガモット (*Citrus bergamia*) をはじめとする汎用性高い機能性食品や化粧品として用いられているものも多数含まれ，医薬品と同様に安全かつ適切な使用が望まれる．

これらの化合物が引き起こす光線過敏症としては，主に(i)狭義の光毒性(phototoxicity)，(ii)光アレルギー性(photoallergy)，(iii)光遺伝毒性(photogenotoxicity)，そして(iv)光発がん性(photocarcinogenicity)があり，毒性発現機序ならびに毒性発現時期がそれぞれ大きく異なっている．なお光毒性については，皮膚反応に限定した場合には光刺激性(photoirritation)と呼ばれる．光毒性や光刺激性は非アレルギー性の急性反応であり，紅斑，小水疱，丘疹，色素沈着等の皮膚の異常反応を特徴とする．一方，光アレルギー性はその名のごとく免疫介在性の毒性反応であり，毒性反応の発現までにやや時間を要する．光遺伝毒性と光発がん性は，化学物質に曝露した後に本来毒性を示さない用量の紫外線あるいは可視光によって惹起される遺伝毒性反応ならびに発がん応答とそれぞれ定義される．

これら光線過敏症の機序として，筆者らが推測しているものを模式的に図1に示した.[5] すなわち，体内に取り込まれた光毒性物質は皮膚組織に到達し，UV曝露によって励起され，その際に励起エネルギーは生体内物質や酸素分子に転移したり，化合物そのものが生体内物質と結合して光付加物を形成する．特に酸素分子との反応によって一重項酸素やスーパーオキシド等の活性酸素種を産生し，それが薬剤性光線過敏症を引き起こす原因の1つとして考えられている．その際に，細胞膜上の各種生体成分を酸化すれば光刺激性を誘発し，また，DNAの酸化あるいは塩基修飾によって光遺伝毒性が発現する．励起された薬物によりタンパク質の光付加物を形成した際には，抗原性が高まり光アレルギー反応を惹起するものと考えられ，薬物が励起された後に反応する分子種によって発現する毒性反応がそれぞれ異なるわけである．薬物の光化学的特性と各種光毒性反応とのより詳細な関連性については，総説を参照されたい.[4]

3　光安全性に関するレギュレーションと創薬へのインパクト

医薬品の光安全性評価に関して，既に欧米の規制当局から数種のガイダンスが提示されている(表2)．2002年に欧州医薬品審査庁(EMEA)／欧州医薬品委員会(CPMP)から，翌年の2003年には米国食品医薬品局(FDA)／医薬品評価研究センター(CDER)からそれぞれガイダンスが示され，

表2　欧米の光安全性評価ガイドライン

ガイドライン	EMEA/CPMP	FDA/CDER	OECD
	guidance on photosafety testing	guidance for industry photosafety testing	*In vitro* 3 T 3 NRU phototoxicity test
対象となる化合物			
対象化合物の範囲	化学物質全般 バイオテクノロジー医薬品	すべての原薬および製剤成分 外用剤は製剤での実施を推奨	UV/VIS 吸収を示す化学物質全般
UV/VIS 吸収特性	290～700 nm モル吸光係数に関する記載なし	290～700 nm モル吸光係数に関する記載なし	290～700 nm モル吸光係数：10 $M^{-1}\cdot cm^{-1}$ 以上
投与経路と体内分布	局所適用 皮膚・眼に到達	皮膚・眼に適用もしくは分布 皮膚・眼に影響を与えるもの	—
評価方法			
光刺激性	3 T 3 NRU phototoxicity test	3 T 3 NRU phototoxicity test マウス，モルモット，ブタ，ウサギを用いた *in vivo* 試験	3 T 3 NRU phototoxicity test
光アレルギー性	改良されたLLNAアッセイやMESTアッセイが将来的に有用になる可能性を示唆するのみ	—	—
光遺伝毒性	光化学的染色体異常誘発性試験 *in vivo* コメット試験 トランスジェニック変異原性モデル	サルモネラ菌，酵母，V 79 細胞を用いた *in vitro* 光遺伝毒性試験	—

2004年には経済協力開発機構(OECD)からより具体性を持った評価方法が提示されている．これら3種のガイドラインの共通点として，化合物の光化学的特性，特に地表に到達する一般的な太陽光の波長領域に相当する290～700 nmの光吸収特性が光毒性と関連することを示唆しており，この波長領域における光吸収測定の必要性が記述されている．これは，1817年に提唱された光化学第一法則(またはGrotthuss-Draper law)の概念である“入射した光のうち，吸収されたものだけが反応に関わる”に即しており，すなわち光吸収する化合物のみが光毒性反応を示し得ることを意味している．

これらのガイドラインでは，一次スクリーニングとして光吸収特性を評価し，光励起されやすい化学物質について更なる生物学的評価を実施することが提案されている．なお，CPMPやCDERガイドラインでは光吸収特性に関する閾値を特に設定していないが，OECDガイドラインでは評価系におけるモル吸光係数に関する閾値を10 $M^{-1}\cdot cm^{-1}$と設定しており，実質的にはすべての化合物を対象として光安全性試験の実施が必要となる．これは創薬において必ずしも小さい負担とは言い難く，それゆえ，より現実的なモル吸光係数を閾値として設定すべく欧米製薬企業を中心に研究が行われている．

この中でHenryらは，35種類の既知光毒性医薬品を対象として290～700 nmの光吸収特性を精査し，経験則的にモル吸光係数1,000 $M^{-1}\cdot cm^{-1}$がより適切な閾値であり，これを超えない医薬品については光安全性評価を実施する必要性は低いことを示している．[6] 光吸収特性の他に物理化学的特性を指標とした一次スクリーニングとしては，光安定性試験やdeductive estimation of risk from existing knowledge(DEREK)を利用したStructural alertなども有用なツールとなる可能性がガイドライン上で提示されており，それらの結果は光安全性試験実施の要否の判断に利用することができる．

これら光化学的知見をもとに，更なる光毒性，光アレルギー，光遺伝毒性／光がん原性試験を実施することとなるが，現段階で最も明確にその試験方法と判断基準について提示されている評価系は，OECDガイドラインの *in vitro* 3 T 3 NRU phototoxicity testである．本アッセイ系は欧州代替法評価センター(ECVAM)によって *in vivo* 試験の代替として開発されたものであり，Balb/c 3 T 3株に対する光照射下の細胞毒性を評価するものである．[7] *In vitro* 3 T 3 NRU phototoxicity testは非常に高感

度な測定系であるため，より安全な医薬候補化合物の創製に大きく寄与することが期待できるが，その反面，高頻度な擬陽性提示とそのデータ取り扱いについてしばしば議論の対象となっている.[3] さらに本評価系では免疫応答反応と遺伝毒性反応を再現することが難しく，結果が必ずしも光アレルギーや光遺伝毒性／光がん原性を反映していない．それゆえ，本試験のみで光安全性を完全には評価することが難しく，データの解釈には創薬従事者に細心の注意を要する．

4 創薬初期過程での光安全性評価

臨床における薬剤性光線過敏症診断としてはphotopatch testや皮膚の生体組織検査等が従来実施され，特に前者は*in vivo*光感作試験として幅広く利用されてきた．一方，創薬においては，簡便に光安全性を評価する方法として先述の*in vitro* 3T3 NRU phototoxicity testが代替試験法として検討されてきた．しかしながら，創薬初期過程ではスクリーニングの更なる高効率化や異なる機序の光線過敏症リスク評価が求められ，これまでにも数多くの評価系が開発・応用されている(表3).[4] これらは，*in silico*スクリーニングツールや光化学的特性を中心とした分子物性評価，あるいは各種毒性反応に特異的な光生物化学的アッセイ方法などが含まれている．これらのアッセイ手法は創薬のステージによってその利用方法や位置付けが異なっており，例えばDEREKやHOMO-LUMO Gap等の*in silico*システムでは，創薬支援として化合物が実際に合成される前段階で新規化合物の光安全性予測を行うことを目的で利用される．一方，光化学的特性評価ツールは実際に合成された医薬候補化合物の分子物性を指標とした光感受性分析を主体とし，必ずしも光安全性を直接的に評価可能なわけではないが，薬剤性光線過敏症の誘発に寄与し得る光化学的反応の有無について高いスループットで示唆することができる．

さて，薬剤性光線過敏症には幾つかの種類が報告されているが，既報の光安全性評価方法はそれらを網羅的に評価するものよりも，むしろ個々の毒性反応に特異的なアッセイ系が多い．その中でも光刺激性評価のためのツールが数多く開発されており，枯草菌，白血球や赤血球を用いたアッセイ系やヒト三次元培養皮膚モデルを利用した評価系が*in vitro*光毒性試験法として有用である．光アレルギー性試験としては国際的に同意が得られた評価系がまだ開発

表3 薬剤性光線過敏症リスク評価のためのアッセイ手法の一例

アッセイ	原理
光化学的特性評価	
UV absorption	Grotthus-Draperの法則に従い，光吸収による励起されやすさ
ROS assay/D-ROM assay	光照射に伴う化合物からの活性酸素種産生
In Silico prediction	
DEREK	毒性既知骨格からの毒性予測
HOMO-LUMO Gap	HOMO/LUMO準位間のエネルギー差算出による光励起されやすさ予測
光毒性／光刺激性評価	
Photopatch test	光刺激性と光アレルギー反応による皮膚の状態変化
Photo-basophil-histamine-release test	白血球からの炎症メディエーター遊離
Photohemolysis model	光毒性反応による赤血球の膜障害
Human reconstituted epidermis model	光毒性反応によるヒト人工皮膚上の形態変化
3T3 neutral red uptake phototoxicity test(3T3 NRU PT)	3T3 mouse fibroblastsを用いた*in vitro*光毒性試験
Oxygen consumption in *Bacillus subtilis*	*Bacillus subtilis*の酸素消費量の変化
光アレルギー性評価	
Pig skin model	ブタ皮膚におけるdrug-protein photoadductの形成
Photo-h-CLAT	Tリンパ球への抗原提示の際における樹状細胞の表面分子発現変化
光遺伝毒性評価	
Capillary gel-electrophoretic DNA-photocleaving assay	光照射に伴うplasmid pBR 322 DNAの高次構造変化
DNA-binding assay	薬物のDNA結合特性とROS産生能による光遺伝毒性リスク評価
Intercalater-based photogenotoxicity assay	Intercalating dyeを用いた光依存的DNA障害評価

されているとはいえないが，ブタ皮膚を用いてdrug-protein photoadductの形成を評価するpig skin modelや，CD 86/54発現亢進を指標としたphoto human cell line activation test(photo-h-CLAT)が現在検討されている．さらに光遺伝毒性試験としては，photo Ames試験が国内外で使用されているが，近年その検出感度が疑問視されている．*In vitro* 光遺伝毒性評価系として，筆者らのグループもキャピラリー電気泳動やDNA intercalaterを利用したアッセイを提案しているが，これらはすべて光励起化合物によるDNA傷害性を指標としたアッセイである．[9~11]

このように創薬初期段階において有用な試験方法にはそれぞれ特徴があり，対象となる光毒性反応やその作用機序，さらに被験物質の物性(溶解性，安定性)も考慮した上で適切な試験法を選定することが重要であろう．また，光化学療法で使用されているγ-アミノレブリン酸はそれ自身は光線過敏を起こさないが，皮膚の病変部に外用すると吸収される過程でポルフィリン体に代謝されて光毒性反応を示す．このような機序を有する医薬品の光安全性評価は*in silico* はもちろん，シンプルな*in vitro* 系でも十分に行うことができず，それゆえ光安全性評価従事者は，各アッセイ系の限界を考慮した上で偽陽性あるいは偽陰性のリスクについても十分な考察が必要とされるであろう．

5 ROSアッセイの開発と応用

薬剤性光線過敏症の機序を考えるとき，最も重要なトリガーとなるのは太陽光の吸収，そしてそれに伴う化合物の励起であろう．しかし，励起されたすべての化合物が一様に光毒性を惹起するわけではなく，図1に示したようにROS産生等の光化学的反応を引き起こす化合物が光毒性を誘発するものと考えられる．この観点から「太陽光の吸収しやすさ」の指標であるUV/VIS吸収特性よりも，むしろ励起エネルギーによる光化学的反応性を直接評価することが，より実質的な光毒性予測に寄与できる可能性がある．

そこで筆者らは，この観点から光照射下における薬物からのROS産生を指標とした新たな光毒性予測ツールであるROSアッセイを2006年に考案した．[5] 既に発売されている複数の医薬品をそれぞれROSアッセイで評価したところ，副作用報告として光線過敏症が報告されている化合物群はROSを産生する傾向にあり，一方，様々なスクリーニングで光安全性の高いと考えられる化合物群からのROS産生は極めて限定されたものであった．すなわち，ROSアッセイは光毒性リスクを予測する上で有用なツールとなる可能性が示唆され，筆者らはこの物性スクリーニング系をHTSに応用することを計画し，スループットの改善とアッセイの小スケール化に成功した．[12,13]

ROSアッセイの利点としては，医薬品の光化学的反応性を迅速かつ簡便に測定できることが挙げられるが，その反面，本アッセイデータは光安全性だけではなく，光安定性などに問題がある化合物も含めて陽性と判別してしまうことが課題の1つである．これはROSアッセイが光化学的反応性評価法であるがゆえの問題点であり，光安全性評価における一次スクリーニングとして本法を利用する際にはこの点を熟考の上，データの解釈をされたい．本ROSアッセイについては，国立医薬品食品衛生研究所，日本製薬工業協会ならびに筆者らを中心として，将来的なガイドラインへの提案を目的とした施設間バリデーションを実施中である．

さて現行のROSアッセイでは，一重項酸素とスーパーオキシドの両方を測定することで総合的に光線過敏症リスクを評価するが，筆者らはROSの代謝物を一度に測定することでよりスループットを向上させ，なおかつ分析に必要な光照射時間を約1分までに短縮したderivative of reactive oxygen metabolites(D-ROM)アッセイを新しい光線過敏症リスク評価方法として2010年に提案した．[14] しかしながら，これら光化学的特性を指標としたアッセイ方法はまだ開発されて時期が浅く，データの解釈とアッセイの位置付けを含めてまだまだ議論の余地が残るところである．今後の継続したデータ蓄積によって実用的な閾値の算出が可能になり，より安全な医薬品創製に貢献できることを強く期待したい．

6 おわりに

薬剤性光線過敏症を回避するための取り組みは欧米を中心として進められており，既に *in vitro* 3T3 NRU phototoxicity test が有用な光毒性試験法として国際的にも広く認知されているものの，国際的に標準化された screening strategy の確立にはまだ至っていないのが現状である．ICH のトピックとして光安全性試験が追加されたこともあり，光安全性についての規制当局の関心は更に高まることが予想される．当然のことながらレギュラトリーサイエンスの観点だけではなく，創薬初期過程においても薬剤性光線過敏症リスクの回避を考えていく必要性がより高まるであろう．包括的な光安全性評価のためには，*in vitro* 光毒性反応とその機序に関する情報だけではなく被験物質の光化学的反応性を中心とした物理化学的特性，皮膚移行性ならびに皮膚滞留性などの薬物動態学的特性を深く精査することも必要である．また現状では，光刺激性に関しては評価系が充実しているが，光アレルギー性や光遺伝毒性／光がん原性評価方法はまだ十分な選択肢があるとはいえない状況である．今後，各種光毒性反応をより特異的かつ高感度に評価可能なリサーチツールと，それらを用いたより適切な screening strategy が提示され，高効率な創薬につながることが期待される．

参考文献

1) Madhukar A. *et al*., *J. Photochem. Photobiol. B : Biol*., 14, 3-22 (1992).
2) Moore D. E., *Mutat. Res*., 422, 165-173 (1998)
3) Moore D. E., *Drug Saf*., 25, 345-372 (2002)
4) Onoue S. *et al*., *Curr. Drug Saf*., 4, 123-136 (2009)
5) Onoue S. *et al*., *Pharm. Res*., 23, 156-164 (2006).
6) Henry B. *et al*., *J. Photochem. Photobiol. B*, 96, 57-62 (2009).
7) Spielmann H. *et al*., *Altex*, 11, 22-31 (1994)
8) Lynch A. M. *et al*., *Exp. Toxicol. Pathol*., in press (2011)
9) Seto Y. *et al*., *J. Pharm. Biomed. Anal*., 52, 781-786 (2010)
10) Onoue S. *et al*., *J. Chromatogr. A*, 1188, 50-56 (2008).
11) Onoue S. *et al*., *J. Pharm. Sci*., 98, 3647-3658 (2009).
12) Onoue S. *et al*., *Pharm. Res*., 25, 861-868 (2008)
13) Onoue S. *et al*., *J. Pharm. Biomed. Anal*., 47, 967-972 (2008)
14) Onoue S. *et al*., *Pharm. Res*., 27, 1610-1619 (2010).

Book Review

新刊紹介

もっとわかる薬物速度論
添付文書の薬物動態パラメーターを読み解く

加藤基浩 著

南山堂／A5・125頁・1,995円

薬物動態学については，薬学部で学んだ人であればAUC，$T_{1/2}$などのパラメーターに関して何となく知っているが，肝心なところはあいまいな気がする，というのが私を含む多くの方の実感ではないだろうか．

本書は，その「何となく」理解している薬物速度論を，一歩踏み込んでより使える知識とすることを目的として，基礎知識の確認とその応用法が記されている．副題にもあるが，特に添付文書の読み方に関して頁を割いて具体的に説明している点が大きな特徴である．

第1章ではなぜ薬物速度論が分かりにくいか，というタイトルでメディシナルケミストや臨床関係者にとって必要となる知識と，その使い方の提案をしている．立場によって必要な情報が異なるのも，薬物速度論の全体像を分かりにくくしている原因であると説き，読者の緊張を解いてくれる．続いて第2章から順に，クリアランス概念やコンパートメントモデルなど基礎知識の解説がある．各章が十数頁前後と手ごろなボリュームにまとめられており，最小二乗法など統計学の基礎概念についても説明があるおかげで，読み進めやすく自然に理解を深めることができる．

最後の第7章が，最も多く頁を割いている添付文書の読み解き方である．簡易評価のための係数相互の関係を示すグラフの助けを借りつつ，基礎的な知識を用いるだけで医薬品の体内動態をここまで添付文書から推測することができるというのは，新鮮な驚きであるとともに病院・薬局の薬剤師の方々には，是非確認しておいてほしいと感じた．

本書は一読の後手元に置いて，必要な際にパラパラと読み返すことで企業の研究者でも活用できそうだ．知識を深めたいと感じている薬学関係者に，幅広く薦めることのできる1冊である．

佐藤康夫　Yasuo SATO

※本書は，日本薬学会「薬学情報コーナー」で閲覧できます．

In Vitro Cell.Dev.Biol.—Animal (2010) 46:774–780
DOI 10.1007/s11626-010-9344-9

Cultured human corneal epithelial stem/progenitor cells derived from the corneal limbus

Naoki Yamamoto · Koji Hirano · Hajime Kojima · Mariko Sumitomo · Hiromi Yamashita · Masahiko Ayaki · Koki Taniguchi · Atsuhiro Tanikawa · Masayuki Horiguchi

Received: 26 March 2010 / Accepted: 19 August 2010 / Published online: 16 September 2010 / Editor: J. Denry Sato

Abstract Stem/progenitor cells of the human corneal epithelium are present in the human corneal limbus, and several corneal epithelial stem/progenitor cell markers have been reported. Recently, the neurotrophin family receptors were reported to be useful markers of corneal epithelial stem/progenitor cells. Therefore, we examined an enzymatic separation method for obtaining corneal epithelial stem/progenitor cells and measuring the change in the expression of low-affinity neurotrophin receptor p75 ($p75^{NTR}$), a receptor belonging to the neurotrophin family. As a result, it was found that our separation method preserved cell viability. Furthermore, $p75^{NTR}$ was mainly observed in epithelial basal cells as were the corneal epithelial stem/progenitor markers p63 and integrin β1. $p75^{NTR}$ was also observed in the cultured cells, but its frequency decreased with passage. In conclusion, we propose that our culture method will enable the culture of corneal stem cells and that it is a useful tool for elucidating the molecular basis of the niche that is necessary for the maintenance of epithelial stem cells in the corneal limbus. Furthermore, we conclude that $p75^{NTR}$ is a useful cell marker for evaluating the characteristics of stem/progenitor cells in culture.

Keywords Human corneal epithelium · Corneal limbus · Low-affinity neurotrophin receptor p75 ($p75^{NTR}$) · p63 · Integrin β1

N. Yamamoto (✉) · M. Sumitomo · H. Yamashita · K. Taniguchi
Laboratory of Molecular Biology and Histochemistry,
Fujita Health University Joint Research Laboratory,
1-98 Dengakugakubo, Kutsukake-cho,
Toyoake, Aichi 470-1192, Japan
e-mail: naokiy@fujita-hu.ac.jp

K. Hirano · A. Tanikawa · M. Horiguchi
Department of Ophthalmology,
Fujita Health University School of Medicine,
1-98 Dengakugakubo, Kutsukake-cho,
Toyoake, Aichi 470-1192, Japan

H. Kojima
Division of Pharmacology, Biological Safety Research Center,
Japanese Center for the Validation of Alternative Methods
(JaCVAM), National Institute of Health Sciences,
1-18-1, Kamiyoga,
Setagaya-ku, Tokyo 158-8501, Japan

M. Ayaki
Department of Ophthalmology,
Showa University Fujigaoka Rehabilitation Hospital,
2-1-1, Fujigaoka, Aoba-ku,
Yokohama 227-8518, Kanagawa, Japan

Introduction

The cornea is comprised of five layers, the corneal epithelium, Bowman's membrane, the corneal stroma, Descemet's membrane, and the corneal endothelium. Several types of non-differentiated cells are present in the corneal epithelium: stem cells with self-replication competence; progenitor cells produced by the asymmetric division of stem cells; and transient amplifying (TA) cells, which are produced by the differentiation of progenitor cells (Qi et al. 2008). As the corneal epithelium is damaged by exposure to ultraviolet rays and oxygen (Higa et al. 2005), it undergoes constant turnover; i.e., TA cells from the basal layer of the corneal epithelium replace the corneal epithelial cells that detach from the surface of the corneal epithelium at a high rate under steady-state conditions. Homeostasis of the corneal epithelium is governed by a small subpopulation of corneal epithelial stem/progenitor cells located in the basal epithelium layer of the limbus. (Qi et al. 2007).

Corneal epithelial stem/progenitor cells, which are very slow-cycling cells (Cotsarelis et al. 1989), move from the limbus to the central region of the cornea, where TA cells are found (Buck 1985).

The low-affinity neurotrophin receptor p75 ($p75^{NTR}$) is one of various markers of self-renewing tissue stem cells (Kunimura et al. 1998; Hahn et al. 2005; Yamamoto et al. 2007), and $p75^{NTR}$-positive cells isolated from human esophageal epithelial cells, such as slow-cycling cells and relatively immature keratinocytes, showed several phenotypic characteristics of tissue stem cells (Okumura et al. 2003).

The purpose of this study is to assess the utility of a cell culture method involving enzyme processing in serum-free medium for evaluating the expression of $p75^{NTR}$ in the corneal limbal epithelium and subcultured cells as a marker of immature/mature human corneal epithelial cells.

Materials and Methods

Human corneal tissue. Human corneal preparations and primary corneal epithelial cells were harvested from three donor eyes independently (Asian; male; age range, 43–56 yr). The donor corneas were obtained from the Northwest Lion Eye Bank (Seattle, WA) in accordance with the provisions of the Declaration of Helsinki for research involving human tissue.

Immunohistochemistry of corneal tissue. A part of the anterior ocular segment including the corneal tissue was fixed in SUPER FIX rapid fixative solution (Kurabo Industries, Osaka, Japan), which is used for morphological research in ophthalmology (for the lens, retina, and so on) (Yamamoto et al. 2008). The cells of the outer layer of the corneal epithelium sometimes become detached when formalin fixative solution is used, which is most commonly used for tissue fixation, but in this study the structure of the eyeball including not only the corneal epithelium but also the corneal stroma, corneal endothelium, ciliary body, and iris was preserved using SUPER FIX rapid fixative solution. Briefly, the corneal tissue was fixed for approximately 60 min, and 3-μm paraffin sections were prepared from the fixed corneal tissue in the usual manner and incubated with anti-human p63 antibody (ready to use, Nichirei corp., Tokyo, Japan), anti-human integrin β1 antibody (1:100, Millipore Corp., Billerica, MA), and anti-human $p75^{NTR}$ antibody (1:100, Alomone Labs Ltd., Israel) for 1 h at 37°C. The secondary antibodies and working dilutions were as follows: Alexa Fluor® 488-labeled anti-mouse goat IgG antibody (for integrin β1 and p63, 1:1,000, Invitrogen Corp., Carlsbad, CA) and Alexa Fluor® 594-labeled anti-rabbit goat IgG antibody (for $p75^{NTR}$, 1:1,000, Invitrogen), which were incubated with the sections for 1 h at 37°C. DAPI (VECTASHIELD H-1200; Vector Laboratories, Burlingame, CA) was used for nuclear staining. A fluorescence microscope (Power BX-51, Olympus, Tokyo, Japan) was used for observation. In addition, the corneal tissue was observed in detail by hematoxylin and eosin (H. E.) staining.

Cell culture. Normal human corneal epithelial (HCE) cells were separated from the corneal limbus of the peripheral corneal region after Descemet's membrane and the corneal endothelium had been removed. The corneal limbus was then cut into eight equal pieces and carefully separated from the underlying stroma using 0.25% collagenase and Accumax (cell aggregate dissociation medium, Innovative Cell Technologies, Inc. San Diego, CA) at 37°C for 30 min (Grant et al. 2005), before being washed twice with phosphate-buffered saline solution (PBS; Sigma, St. Louis, MO) and diluted ten times in the cell-lotion solution (JUJI FIELD Inc., Tokyo, Japan) using a low-adhesion cell centrifuge tube (Stemful, SUMITOMO BAKELITE Co., Ltd., Tokyo, Japan). In addition, we compared our method with the standard method; i.e., using dispase at 37°C for 60 min (Koizumi et al. 2002; Touhami et al. 2002; Nakamura et al. 2006). The HCE cells were cultured in serum-free PCT corneal epithelium medium (CnT-20 medium, CELLnTEC Advanced Cell Systems, Bern, Switzerland) supplemented with 50 units/ml penicillin and 50 μg/ml streptomycin (Sigma, St. Louis, MO) at 37°C in a 5% CO_2-humidified incubator (Chirila et al. 2008).

To compare the culture conditions, the HCE cells were cultured in a 35-mm culture dish (BD Biosciences, San Jose, CA) (1×10^4 cells/dish) coated with collagen (TOYOBO Co., Ltd., Osaka, Japan) or FNC Coating Mix® (FNC; cell attachment improvement media, Athena Environmental Sciences, Inc., Baltimore MD) (Engler et al. 2009) in CnT-20 medium, and the cells were then subcultured with TrypLE™ Select (Cell dissociation reagents, Invitrogen) (Li et al. 2008) or trypsin (Kurabo industries LTD).

Frozen cultured human corneal epithelial cells (HCEC-2 cells), at passage 2, were purchased from Kurabo industries LTD (Osaka, Japan). The cells were then thawed and cultured in a 35 mm culture dish coated with FNC in EpiLife™ KG2 medium (Kurabo); M-stars C medium, which includes fetal bovine serum (ArBlast Co., Ltd., Hyogo, Japan); or CnT-20 medium, supplemented with antibiotics at 37°C in a 5% CO_2-humidified incubator. Each medium was changed every 2 d, and the cells were subcultured with TrypLE™ Select.

Immunofluorescence staining and flow cytometric analysis. The cells separated from the corneal tissue, the fixed

HCE cells cultured at passage 2 or 4, and the HCEC-2 cells cultured at passage 1 were incubated with anti-human p63 antibody, anti-human integrin β1 antibody, anti-human $p75^{NTR}$ antibody, anti-human TrkA antibody (1:100, Santa Cruz Biotechnology, Inc., Santa Cruz, CA), and anti-human keratin 3 (cytokeratin 3) antibody (1:100, ENZO Life Sciences International, Inc., Farmingdale, NY) at 4°C for 30 min. The cells were then washed with PBS and incubated with the Alexa Fluor® 488-labeled secondary antibody at 4°C for 30 min. Next, the cells were washed with PBS and then observed under a fluorescence microscope or subjected to flow cytometry (fluorescence-activated cell sorting (FACS), FACSCan, BD Biosciences). All experiments were performed three times.

Results

Marker expression in the corneal limbal region. Pigment was observed in the corneal limbal region, which contains corneal epithelial stem/progenitor cells (Fig. 1*A*). The corneal limbal preparation demonstrated melanocytes containing melanin near to the basal region of the corneal epithelium during H. E. staining (Fig. 1*B*). These cells were slightly smaller and demonstrated a higher cell density than their neighboring cells (Fig. 1*C*). The p63 and integrin β1-positive cells were mainly found in the corneal epithelial basal cell layer, and these cells were also positive for $p75^{NTR}$. However, the cells on the surface of the corneal epithelium in the corneal limbus were negative for these markers (Fig. 1*D*–*I*).

Comparison of culture conditions. After 7 d culture, most of the non-coated culture dishes HCE cells were not attached (Fig. 2*A*). However, in the dishes coated with collagen, the HCE cells multiplied to $2.1\pm0.2\times10^5$ from 1×10^4 cells/dish (Fig. 2*B*). Furthermore, in the dishes coated with FNC, the HCE cells multiplied to $3.0\pm0.2\times10^5$ from 1×10^4 cells/dish (Fig. 2*C*). During the cell passage, most of the HCE cells were not attached when trypsin was used (Fig. 2*D*), but the HCE cells multiplied to $3.0\pm0.2\times10^5$ from 1×10^4 cells/dish when TrypLE™ Select was used (Fig. 2*E*). When corneal epithelial cells were separated from the corneal limbus using the standard method, keratocytes were often mixed in with them (Fig. 2*F*).

Morphology of HCE cells. The commercial HCEC-2 cells were distorted at passage 2 regardless of whether they were cultured in EpiLife™ KG2 serum-free medium or M-Stars C. Cell growth arrested at passage 3, and the HCEC-2 cells could not be subcultured after passage 3. In CnT-20 medium, the HCEC-2 cells maintained their form until passage 3, but they could not be subcultured after passage 4. On the other hand, the HCE cells reproduced aggressively at passage 3, and their polygonal form was

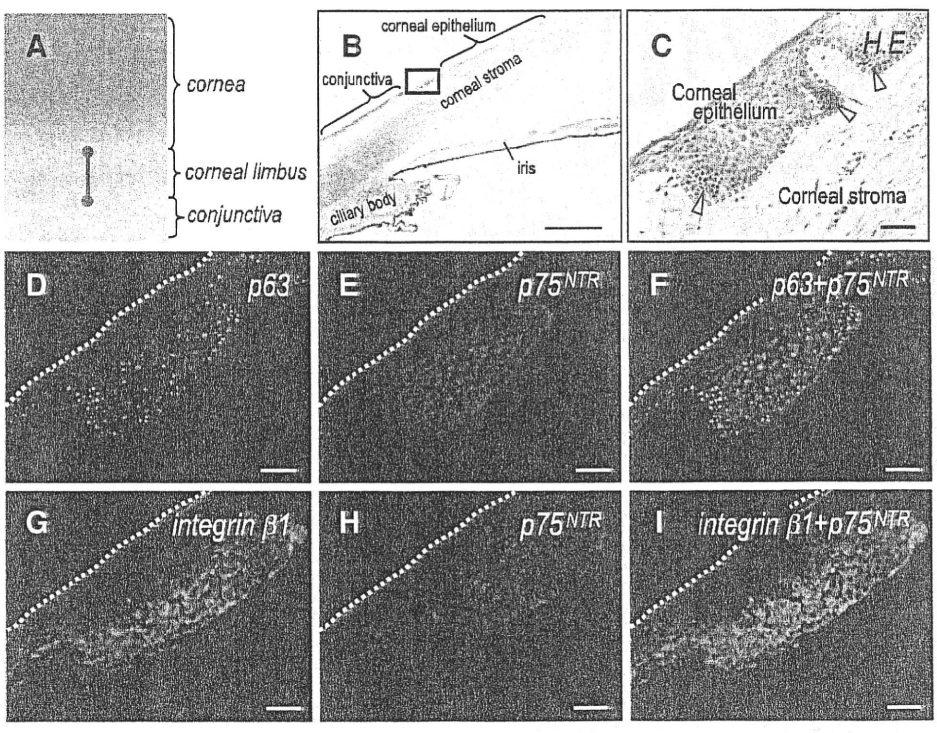

Figure 1 The structure shown (palisades of Vogt) is present in the corneal limbus between the cornea and conjunctiva (*A*). Sections of the human anterior ocular segment were stained with H. E. (*B*, the *bar* indicates 1 mm), and the area in the *black square* has been highly magnified in (*C*). The corneal limbus demonstrated melanocytes (*arrowheads*) containing melanin near the basal region (*green dotted line*) of the corneal epithelium. Staining of the corneal limbus with three antibodies to stem/progenitor markers; p63 (*D*), $p75^{NTR}$ (*E*, *H*), integrin β1 (*G*), merged image of p63 and $p75^{NTR}$ (*F*), and merged image of integrin β1 and $p75^{NTR}$ (*I*). The surface of the corneal epithelium is highlighted by a *white dotted line*. The *bars* indicate 50 μm.

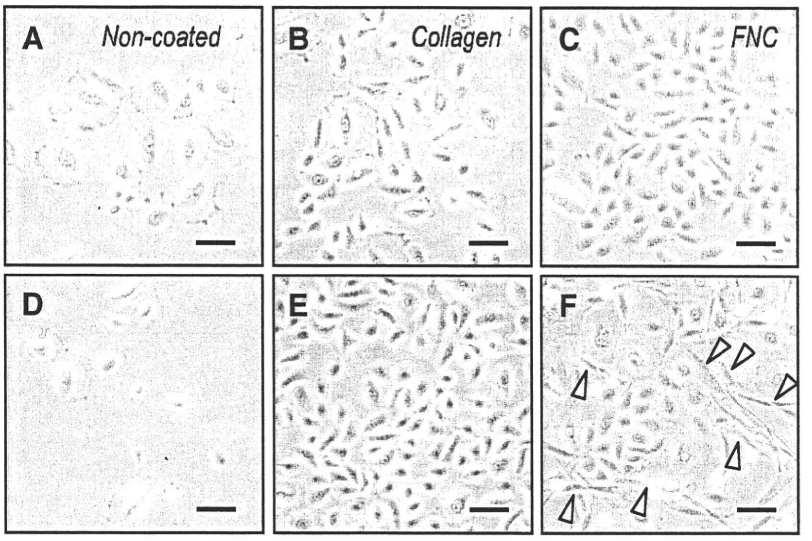

Figure 2 Comparison of culture condition. Most of the HCE cells in the non-coated culture dishes were not attached (*A*). The HCE cells grew more rapidly in the dishes coated with FNC (*C*) than in those coated with collagen (*B*). During the cell passage, most of the HCE cells did not attach when trypsin was used (*D*), but they did attach and grow when TrypLE™ Select was used (*E*). When the standard method was used, keratocytes (*arrowheads*) were often mixed in with the HCE cells (*F*). The *bars* indicate 100 μm.

maintained until passage 4 in CnT-20 medium. However, at passage 6, they became hypertrophic or extended (Fig. 3).

The change in marker expression with passage. The cells separated from the corneal limbus were stained with each antibody, and were counted the number of positive cells under a fluorescence microscope. We found that p63-positive cells accounted for 40.4±2.1% (Fig. 4*A*), integrin β1-positive cells for 34.4±2.0% (Fig. 4*C*), $p75^{NTR}$-positive cells for 28.4±3.1% (Fig. 4*E*), TrkA-positive cells for 24.8±3.2% (Fig. 4*G*), and keratin-positive cells for 70.3±2.7% (Fig. 4*I*) of all cells. Of the HCEC-2 cells, we found that p63-positive cells accounted for 0.7±0.5%, integrin β1-positive cells for 97.1±2.0%, $p75^{NTR}$-positive cells for 3.3±1.2%, TrkA-positive cells for 8.3±1.5%, and keratin-positive cells for 98.3±2.7% (data not shown).

The proportions of cultured HCE cells expressing these markers at passages 2 and 4 were analyzed using FACS.

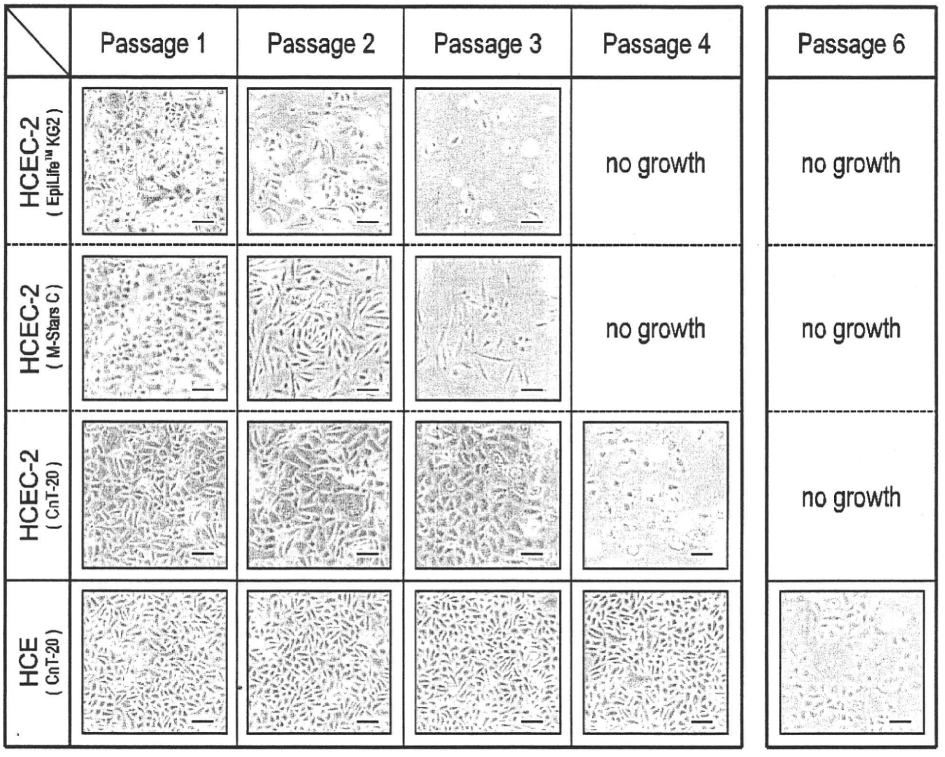

Figure 3 Morphology of HCEC-2 cells and HCE cells. The HCEC-2 cells became distorted cells from passage 2 onwards when cultured in EpiLife™ KG2 medium or M-Stars C medium, but they maintained their form until passage 3 when cultured in CnT-20 medium. On the other hand, the HCE cells reproduced aggressively at passage 3 and maintained their polygonal cell form until passage 4, but their form changed at passage 6. The *bars* indicate 100 μm.

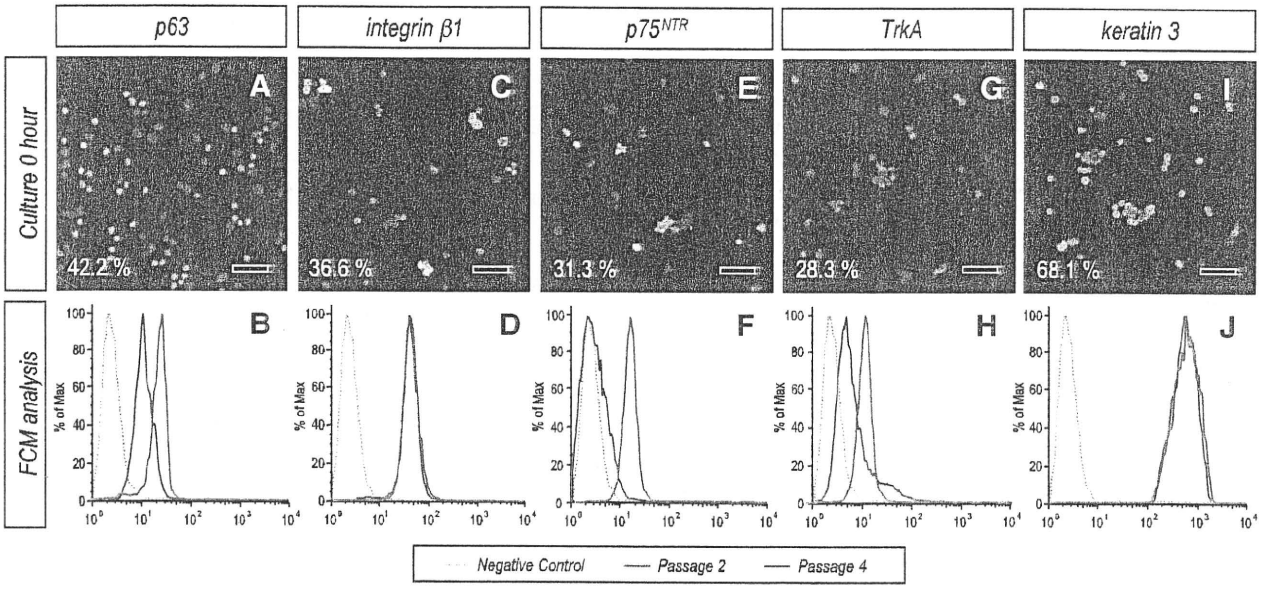

Figure 4. The changes in marker expression with passage. The corneal epithelial stem/progenitor cell markers p63 (*A*), integrin β1 (*C*), $p75^{NTR}$ (*E*), and TrkA (*G*), and the differentiated corneal epithelium cell marker keratin 3 (*I*) were observed in the corneal limbus separated cells. Therefore, the cultured HCE cells were analyzed for p63 (*B*), integrin β1 (*D*), $p75^{NTR}$ (*F*), TrkA (*H*), and keratin 3 (*J*) by FACS at passages 2 and 4. The numbers of p63, $p75^{NTR}$, and TrkA-positive cells were decreased at passage 4. The *bars* indicate 100 μm.

p63-positive cells accounted for 78.6±2.4% of the cells at passage 2 and 49.6±4.7% of those at passage 4 (Fig. 4*B*), and the integrin β1-positive cells accounted for 98.7±0.4% and 97.0±1.1% (Fig. 4*D*), the $p75^{NTR}$-positive cells accounted for 70.2±5.0% and 7.8±0.8% (Fig. 4*F*), the TrkA-positive cells accounted for 85.5±5.3% and 23.8±2.0% (Fig. 4*H*), and the keratin 3-positive cells accounted for 98.6±0.5% and 98.2±0.5% of the cells at passages 2 and 4, respectively (Fig. 4*J*). The numbers of integrin β1 and keratin 3-positive cells were not affected by passage number.

Discussion

Characteristics of the corneal limbus region. Several studies have reported that corneal epithelial stem/progenitor cells are present in the corneal limbus; where limbal papillary structures (palisades of Vogt) are located (Schermer et al. 1986; Cotsarelis et al. 1989; Higa et al. 2005; Li et al. 2007). It is considered that the stem cell niche model applies to the corneal limbus because the melanocytes in the corneal limbus are smaller than the nearby non-melanin cells (Li et al. 2007), adhere to each other, and are attached to corneal epithelial stem/progenitor cells through N-cadherin (Hayashi et al. 2007). Corneal limbus cells were also found to be positive for p63, a known corneal epithelial stem/progenitor cell marker; integrin β1 (CD29) (Nakamura et al. 2006; Liu et al. 2007; Utheim et al. 2009), which is an epithelial stem/progenitor cell marker; and $p75^{NTR}$ (CD271), which is expressed by basal cells (TA cells) but not by cell that have differentiated from TA cells in the center of cornea (Qi et al. 2007; Yamamoto et al. 2007; Qi et al. 2008). The expression of these cell markers was localized to the basal region of the corneal epithelium (no such expression was found for the cells on the surface of the corneal limbus), an extremely unique region in which stem/progenitor cells, TA cells, and differentiated corneal epithelial cells are found.

The separation and culture method. In previous reports, two types of separation method have generally been used to obtain cells from the corneal limbus, an explant method in which the cells were cultured from a small sample of corneal limbus tissue (Kim et al. 2004; Liu et al. 2007; Qi et al. 2008) and an enzymatic method that involved using dispase for 60 min (Koizumi et al. 2002; Touhami et al. 2002; Nakamura et al. 2006). Using our method, corneal epithelial stem/progenitor cells were effectively separated from the corneal limbus by 30-min enzyme processing without keratocyte contamination. Furthermore, in the subculture stage, the adhesive properties of the cells and their viability were improved by using TrypLE™ Select rather than trypsin. In addition, the polygonal form of the cells was maintained until passage 4.

The expression of several markers. In the cells separated from the corneal limbus, $p75^{NTR}$ was expressed in approximately similar proportions to p63, integrin β1, and TrkA (Di Girolamo et al. 2008; Utheim et al. 2009). Furthermore, the corneal epithelial stem/progenitor cells also expressed p63 and ABCG2 (data not shown), but they did not express keratin 3 (Schermer et al. 1986; Cotsarelis et al. 1989; Chen et al. 2004; Hayashi et al. 2007). On the other hand, keratin 3-positive cells were observed at an approximately similar ratio to the stem/progenitor marker negative cells (Qi et al. 2008). As the number of cells expressing p63 and $p75^{NTR}$ decreased with each passage, we concluded that the cultured cells were gradually differentiating into mature corneal epithelial cells. Therefore, because the number of cells expressing integrin β1 on the basal membrane side did not change, we concluded that the adhesion culture method rather than the three-dimensional culture method was the most appropriate for these cells.

The expression of neurotrophin factor receptor. In the cultured cells, we found that the nerve growth factor (NGF) receptor was expressed together with the NGF high-affinity receptor TrkA and the NGF low-affinity receptor $p75^{NTR}$. It is believed that co-expression of the $p75^{NTR}$ and Trk receptors leads to NT signaling through Trk receptors and the promotion of cell survival (Carter and Lewin 1997; Dechant and Barde 1997). The neurotrophin family consists of four members: NGF, brain-derived neurotrophic factor, neurotrophin-3 (NT-3), and neurotrophin-4/5 (NT-4/5), and NT-3 and NT-4/5 have a sequence homology of at least 50%. A neurotrophin is a kind of cytokine that is involved in maintaining the viability of nerves (Johansson et al. 1997), the promotion of axis regeneration (Hollowell et al. 1990), and the growth and development of the regeneration-promoting nervous system (Levi-Montalcini and Booker 1960). The receptors for this neurotrophin family are molecules of the Trk family of tyrosine kinase receptors: NGF has a high affinity for Trk A, BNDF and NT-4/5 have high affinities for Trk B, and NT-3 has a high affinity for Trk C. $p75^{NTR}$ can bind to all four of these neurotrophins (Bothwell 1995; Bibel et al. 1999; Dechant 2001) and has recently been renamed CD271.

Finally, a report about the signals relevant to the embryonic stem cell niche was recently published (Bendall et al. 2007). We expect that our findings will enable the elucidation of the molecular basis of the niche that is necessary for the maintenance of epithelial stem cells for researching the corneal limbus. Therefore, we conclude that $p75^{NTR}$ is a cell marker that can be used to evaluate the characteristics of stem/progenitor cells produced using the adhesion culture method.

Acknowledgments This study received public welfare labor science research expenses subsidies (H19-medicine public-003: from 2007 to 2009, and H22-medicine public-002: from 2010 to 2012) and assistance from the Ministry of Education, Culture, Sports, Science, and Technology in the form of Grants in Aid for Scientific Research JAPAN (19700324 and 22591970).

References

Bendall S. C.; Stewart M. H.; Menendez P.; George D.; Vijayaragavan K.; Werbowetski-Ogilvie T.; Ramos-Mejia V.; Rouleau A.; Yang J.; Bossé M.; Lajoie G.; Bhatia M. IGF and FGF cooperatively establish the regulatory stem cell niche of pluripotent human cells in vitro. *Nature* 448: 1015–1021; 2007. doi:10.1038/nature06027.

Bibel M.; Hoppe E.; Barde Y. A. Biochemical and functional interactions between the neurotrophin receptors trk and p75NTR. *EMBO J* 18: 616–622; 1999. doi:10.1093/emboj/18.3.616.

Bothwell M. Functional interactions of neurotrophins and neurotrophin receptors. *Ann Rev Neurosci* 18: 223–253; 1995. doi:10.1146/annurev.ne.18.030195.001255.

Buck R. C. Measurement of centripetal migration of normal corneal epithelial cells in the mouse. *Invest Ophthalmol Vis Sci* 26: 1296–1299; 1985.

Carter B. D.; Lewin G. R. Neurotrophins live or let die: does p75NTR decide? *Neuron* 18: 187–190; 1997. doi:10.1016/S0896-6273(00)80259-7.

Chen Z.; de Paiva C. S.; Luo L.; Kretzer F. L.; Pflugfelder S. C.; Li D. Q. Characterization of putative stem cell phenotype in human limbal epithelia. *Stem Cells* 22: 355–366; 2004. doi:10.1634/stemcells.22-3-355.

Chirila T.; Barnard Z.; Zainuddin; Harkin D. G.; Schwab I. R.; Hirst L. Bombyx mori silk fibroin membranes as potential substrata for epithelial constructs used in the management of ocular surface disorders. *Tissue Eng Part A* 14: 1203–1211; 2008.

Cotsarelis G.; Cheng S. Z.; Dong G.; Sun T. T.; Lavker R. M. Existence of slow-cycling limbal epithelial basal cells that can be preferentially stimulated to proliferate: implications on epithelial stem cells. *Cell* 57: 201–209; 1989. doi:10.1016/0092-8674(89)90958-6.

Dechant G. Molecular interactions between neurotrophin receptors. *Cell Tissue Res* 305: 229–238; 2001. doi:10.1007/s004410100378.

Dechant G.; Barde Y. A. Signalling through the neurotrophin receptor p75NTR. *Curr Opin Neurobiol* 7: 413–418; 1997. doi:10.1016/S0959-4388(97)80071-2.

Di Girolamo N.; Sarris M.; Chui J.; Cheema H.; Coroneo M. T.; Wakefield D. Localization of the low-affinity nerve growth factor receptor p75 in human limbal epithelial cells. *J Cell Mol Med* 12: 2799–2811; 2008. doi:10.1111/j.1582-4934.2008.00290.x.

Engler C.; Kelliher C.; Speck C. L.; Jun A. S. Assessment of attachment factors for primary cultured human corneal endothelial cells. *Cornea* 28: 1050–1054; 2009.

Grant A.; Palzer S.; Hartnett C.; Bailey T.; Tsang M.; Kalyuzhny A. E. A cell-detachment solution can reduce background staining in the ELISPOT assay. *Methods Mol Biol* 302: 87–94; 2005.

Hahn C. G.; Han L. Y.; Rawson N. E.; Mirza N.; Borgmann-Winter K.; Lenox R. H.; Arnold S. E. In vivo and in vitro neurogenesis in human olfactory epithelium. *J Comp Neurol* 483: 154–163; 2005. doi:10.1002/cne.20424.

Hayashi R.; Yamato M.; Sugiyama H.; Sumide T.; Yang J.; Okano T.; Tano Y.; Nishida K. N-Cadherin is expressed by putative stem/progenitor cells and melanocytes in the human limbal epithelial stem cell niche. *Stem Cells* 25: 289–296; 2007. doi:10.1634/stemcells.2006-0167.